Earth and Planetary Science Letters 361 (2013) 504–517

Contents lists available at SciVerse ScienceDirect

Earth and Planetary Science Letters

journal homepage: www.elsevier.com/locate/epsl

Retroarc deformation and exhumation near the end of the Andes, southern Patagonia

Julie C. Fosdick [a,*], Marty Grove [a], Jeremy K. Hourigan [b], Mauricio Calderón [c]

[a] Geological & Environmental Sciences, Stanford University, Stanford, CA 94305, USA
[b] Earth Sciences, University of California, Santa Cruz, CA 95064, USA
[c] Departamento de Geología, Universidad de Chile, Casilla 13518, Correo 21, Santiago, Chile

ARTICLE INFO

Article history:
Received 21 June 2012
Received in revised form
3 December 2012
Accepted 3 December 2012
Editor: T.M. Harrison
Available online 29 December 2012

Keywords:
Patagonian Andes
(U–Th)/He thermochronology
exhumation
retroarc thrust-belt
climate

ABSTRACT

The southern Patagonian Andes constitute the narrow, high-latitude end of the Andean orogen belt in South America, where inherited basin paleogeography, subduction processes, retroarc crustal thickening, and late Cenozoic glaciation have collectively influenced their unusual tectonic and physiographic evolution. New zircon and apatite (U–Th)/He thermochronology from the Patagonian Andes between 50°30′ and 51°30′S suggest concentrated exhumation across the retroarc (leeward) side of the orogen since early Miocene time. Zircon (U–Th)/He (ZHe) ages range from 44 to 10 Ma; oldest ages are recorded in the Patagonian batholith and along the far eastern frontal foreland monocline. Regionally-uniform ZHe ages between 22 and 18 Ma, located across a ~75 km wide-zone of the Patagonian retroarc thrust-belt indicate widespread early Miocene cooling through the ZHe partial retention zone. Mesozoic sedimentary and volcanic rocks in this region have been exhumed from at least 5 to 6 km depths. Early Miocene denudation of the thrust-belt, deformation, and increased foreland sedimentation rates coincided with opening of the Scotia Sea, suggesting a causal response of the foreland to changes in plate dynamics. The apatite (U–Th)/He (AHe) ages from a similar region range from 11 to 3 Ma; the youngest ages (6–3 Ma) are spatially clustered within the more deeply-exhumed central thrust domain. We interpret these AHe ages to record > 1–2 km of erosional denudation associated with late Cenozoic glaciation and fluvioglacial processes in Patagonia beginning ca. 7 Ma.

Zircon results indicate that since ca. 22 Ma, long-term exhumation rates have been highest across the western and central thrust domains (0.22–0.37 mm yr^{-1}), and significantly lower along the eastern thrust front (0.10–0.17 mm yr^{-1}). Since ~7 Ma, apatite results from these same regions suggest comparable and slightly higher denudation rates (0.14–0.46 mm yr^{-1}), particularly within the eastern thrust domain, consistent with efficient erosional processes acting in the retroarc region. These results from the Patagonian retroarc region, particularly the predominance of < 7–4 Ma AHe ages, provide a new understanding for regional orogenic erosion models that are largely based on existing data from the windward regions. We suggest that retroarc denudation was enhanced by widespread Miocene structural uplift and unroofing of the fine-grained siliciclastic rocks of the marine Cretaceous Magallanes/Austral foreland basin. Furthermore, its location at the southern tip of the orogen, may have allowed additional moisture to reach the leeward side, leading to sustained late Cenozoic erosional denudation.

1. Introduction

The topographic development of mountain belts in convergent settings is modulated by the interactions between tectonic deformation and surface processes. Crustal thickening caused by batholith emplacement and thrusting build topography while mass removal by erosion and tectonic redistribution via extensional processes reduce it. Numerous studies highlight the importance of erosion on influencing strain distribution, thrust belt morphology, and patterns of rock exhumation (e.g., Dahlen and Suppe, 1988, Beaumont et al., 1992; Brandon et al., 1998; Horton, 1999; Willett, 1999; Wobus et al., 2003; Cruz et al., 2008; Willett and Brandon, 2002). Spatial and temporal variation in erosion rate are key observable parameters that can be related to internal deformation patterns within an orogenic wedge (Davis et al., 1983; Dahlen, 1984; Willett et al., 1993; Koons et al., 2002; Hilley and Strecker, 2004). Moreover, the correlation between erosion rate and mean annual precipitation indicates that large-scale climate patterns can also strongly respond to the physiography of mountain belts and influence internal deformation within them (e.g., Montgomery et al., 2001; Zeitler, 1985; Horton, 1999; Reiners et al., 2003; Thiede et al., 2005; Uba et al., 2009). For instance,

* Corresponding author.
E-mail address: jfosdick@email.arizona.edu (J.C. Fosdick).

0012-821X/$ - see front matter © 2012 Elsevier B.V. All rights reserved.
http://dx.doi.org/10.1016/j.epsl.2012.12.007

orogenic belts that are situated orthogonal to the prevailing wind direction act as orographic barriers to moisture, resulting in a rain shadow with high precipitation and erosion rates on the windward side and low precipitation and erosion rates on the leeward side (e.g., Roe, 2005; Stern and Blisniuk, 2002; Reiners et al., 2003). Numerical modeling predicts that the spatial distribution of exhumation, thrusting, and location of the topographic crest are sensitive to erosional intensity (e.g., Koons, 1989; Willett, 1999; Poage and Chamberlain, 2002; Cruz et al., 2010). Similarly, in glaciated orogenic wedges, complex patterns of glacial excavation affect the morphology and spatial patterns of deformation and exhumation (Tomkin, 2007; Tomkin and Braun, 2002; Berger and Spotila, 2008; Thomson et al., 2010).

While relationships between crustal deformation and surface processes are becoming increasingly well-understood in convergent settings, much of what is known has been learned from the central portions of orogenic systems which exhibit the thickest crust and the highest elevations (e.g., Willett, 1999; Horton, 1999; Barnes et al., 2008, 2012; McQuarrie et al., 2008; Thiede et al., 2005). Far less attention has been paid to the narrow ends of orogenic belts where large-scale mountain systems terminate. There, the along-strike deterioration of high topography, changes in lithospheric strength, plate boundary interactions, and variable lithology can affect the behavior of orogenic exhumation and deformation.

Southern Patagonia, situated at the high-latitude end of the Andean Cordillera, north of the Drake Passage, offers an excellent setting for examining interactions between tectonic deformation and surface processes where a continent narrows to a more readily deformed and exhumed orogenic wedge (Fig. 1). Since at least middle Miocene time (Blisniuk et al., 2005), and possibly as early as the Eocene opening of Drake Passage (Eagles et al., 2005; Livermore et al., 2007; Barbeau et al., 2009; Lagabrielle et al., 2009), the Patagonian Andes have been situated orthogonal to the moisture-bearing southern hemisphere westerlies, giving rise to a strong precipitation gradient across the orogen (Fig. 1) (Strecker et al., 2007). In the leeward retroarc region, crustal shortening and growth of the Patagonian fold-and-thrust belt commenced in Late Cretaceous time, though significant Cenozoic structural shortening (Kraemer, 2003) and Miocene deep-seated thrusting has accommodated crustal thickening and widening of the orogenic wedge (Harambour, 2002; Radic et al., 2007; Fosdick et al., 2011). More recently, the Patagonian Andes underwent significant changes in climate regime with late Cenozoic glaciation and expansion of the Patagonian ice sheet (Mercer and Sutter, 1982; Zachos et al., 2001; Rabassa et al., 2005; Kaplan et al., 2009).

This orographic configuration is considered a 'wet prowedge' (cf. Willett, 1999), for which numerical modeling predicts maximum exhumation within the orogen interior on the windward side of the mountain belt and migration of the topographic divide toward the retroforeland (Willett, 1999; Cruz et al., 2008). Regional low-temperature thermochronology from the Patagonian Andes depict an eastward migration of maximum denudation (Thomson et al., 2001; Thomson, 2002). Additionally, these data characterize a pronounced along-strike gradient in magnitude of exhumation interpreted as a poleward decrease in Late Cenozoic erosional efficiency by glaciers (Thomson et al., 2010). Southward, however, few of these data capture the exhumation record on the retrowedge (leeward) side of the orogenic belt, motivating further inquiry into orogenic exhumation and deformation patterns across the whole southern Patagonian orogenic belt.

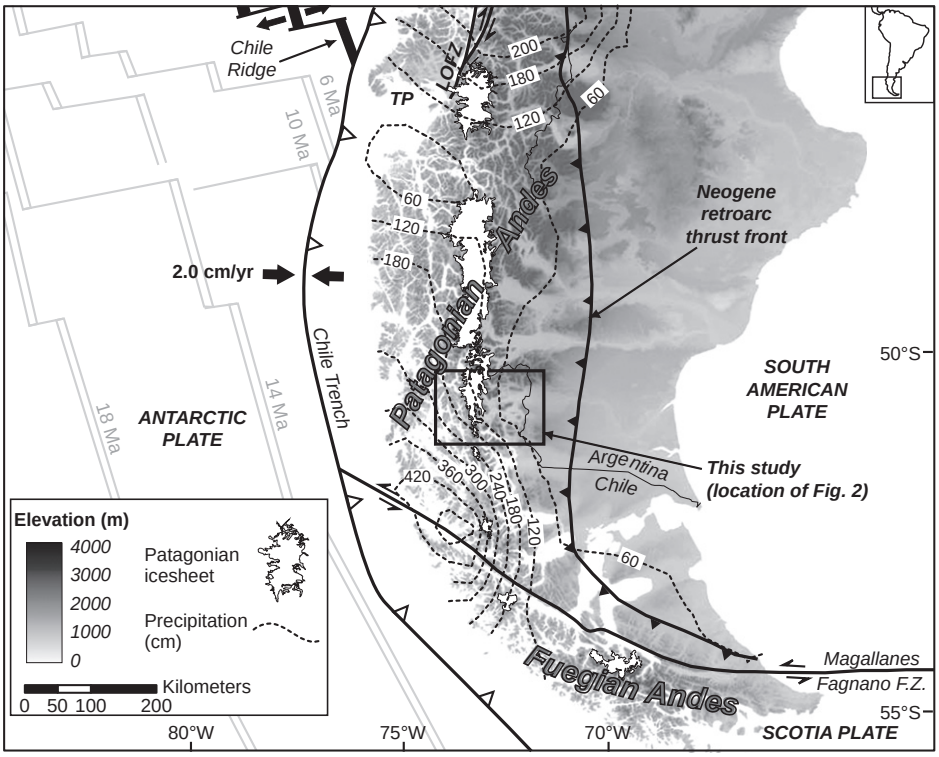

Fig. 1. Tectonic and physiographic setting of the study area (black box) in the southern Patagonian Andes showing relationships between the Antarctic, South American, and Scotia plates. The active Chile spreading ridge intersects the Chile Trench at the Taitao Peninsula (TP) and paleoreconstructions of its position with respect to the South American margin are indicated by gray lines (after Cande and Leslie (1986)). The position of the retroarc thrust front is drawn from Ramos (1989), Klepeis (1994), and Fosdick et al. (2011). High topography exists along the crest of the Patagonian Andes and mountain elevations decrease southward. White star indicates the location of published paleoaltimetry study of Blisniuk et al. (2005). LOFZ=Liquiñe-Ofqui fault zone after Cembrano et al. (2000). Precipitation contours plotted from Legates and Willmott (1990). Digital Elevation Model was generated from SRTM 90-m data.

Detailed constraints on the timing and magnitude of long-term erosional flux are critical for understanding how exhumational processes control and respond to tectonic events in orogenic belts. Thermochronology conveys information about the redistribution of heat in the Earth's crust and provides an indirect means of quantifying rock cooling and inferred crustal exhumation (Ehlers and Farley, 2003). Within the context of a convergent orogenic belt, thrusting-induced erosional denudation can be recorded by thermochronometers with mid-crustal temperature sensitivities (e.g., 150–200 °C for zircon (U–Th)/He) (e.g., Lock and Willett, 2008; Metcalf et al., 2009). In contrast, the lower temperature apatite (U–Th)/He system (40–70 °C) is also sensitive to surface processes—such as erosion and sedimentation—and the form of the earth's surface (e.g., Reiners and Brandon, 2006). This study reports apatite and zircon (U–Th)/He thermochronology from the southern Patagonian Andes (Fig. 2) that quantifies the distribution of crustal exhumation and elucidates potential links between tectonic events and erosional denudation at the southern end of the Andean orogenic belt.

2. Tectonic setting

The southern Patagonian Andes constitute a convergent orogenic belt associated with the subduction of the oceanic Nazca, Antarctica, and Scotia plates beneath the overriding and southward-narrowing South American plate (Fig. 1). At the latitude of the study area between 50°30′ and 51°30′S, the present-day margin is characterized by a low convergence rate (~20 mm yr^{-1}), steeply subducting oceanic crust, a narrow accretionary wedge, subduction erosion, and oblique transpression within a segmented forearc basin (Cande and Leslie, 1986; Polonia et al., 2007).

Within the field area, the Patagonian thrust-belt involves variably deformed fine-grained siliciclastic deposits of the Mesozoic Rocas Verdes–Magallanes Basin (Katz, 1963; Dalziel et al., 1974; Wilson, 1991; Fildani and Hessler, 2005; Romans et al., 2011). Overall, we recognize five main lithotectonic domains based on both the magnitude and style of deformation and stratigraphic age of the siliciclastic rocks within the thrust sheets (e.g., Kraemer, 1998) (Fig. 2). From west to east these domains are: (1) the Patagonia batholith that includes Jurassic–Neogene calc-alkaline plutons and Paleozoic metasedimentary wall rocks (Hervé et al., 2003, 2007a; Fanning et al., 2011); (2) the western thrust domain that consists of the Sarmiento ophiolitic complex and volcanogenic Tobífera Formation of the Late Jurassic–Early Cretaceous Rocas Verdes backarc basin (Allen, 1982; Calderón et al., 2007, 2012); (3) The central thrust domain, which exposes strongly deformed Aptian–Turonian strata of the Magallanes foreland basin and isolated exposures of the underlying Upper Jurassic volcaniclastic succession; (4) the eastern thrust domain that consists of open folding and minor thrust faulting within Coniacian–Maastrichtian

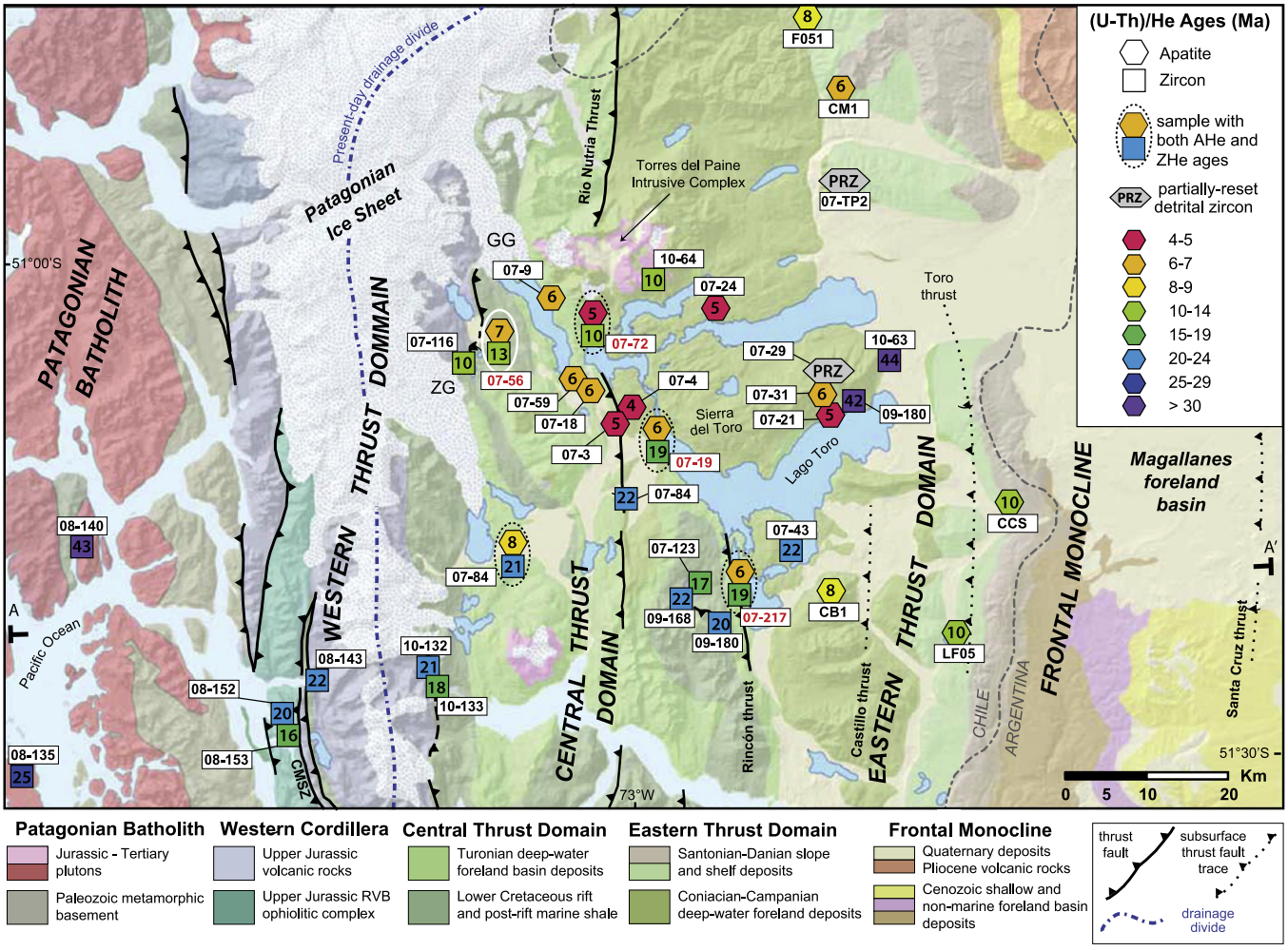

Fig. 2. Thermochronology results from the Patagonian Andes between 50°30′S and 51°30′S. Apatite (hexagons) and zircon (squares) correspond to weighted mean (U–Th)/He ages and are color-coded by age. Geology modified from Fosdick et al. (2011) and references therein. BGC=Balmaceda granitic complex, TPIC=Torres del Paine Intrusive Complex, GG=Gray Glacier, ZG=Zapata Glacier. Blue dashed line defines position of present-day drainage divide. Cross-section line A–A′ is shown in Fig. 3.

foreland basin-fill (Wilson, 1991; Harambour, 2002; Fosdick et al., 2011); and (5) the frontal monocline which contains Paleocene–Miocene foreland basin sediments.

The Magallanes foreland basin was an elongate trough that formed in response to retroarc convergence and closure of the Rocas Verdes backarc basin (Dalziel et al., 1974; Wilson, 1991; Fildani and Hessler, 2005). Retroforeland shortening initiated in our study area at ca. 100 Ma and produced a well-developed subaerial retroforeland thrust-belt that provided sediment to the deep-marine foredeep depocenter by 92 Ma (Fildani et al., 2003; Fosdick et al., 2011). The basin was progressively filled with predominantly deep-marine sediments and overlying shallow-marine and fluvial-deltaic deposits (Natland et al., 1974; Malumián and Caramés, 1997; Hubbard et al., 2008; Covault et al., 2009). Significant crustal shortening occurred across the thrust-belt during Late Cretaceous time (100–88 Ma), followed by an episode of Paleogene shortening responsible for thin-skinned deformation of the Upper Cretaceous foredeep sediments (Fig. 2) (Kraemer, 1998; Klepeis et al., 2010). Miocene regional retroforeland uplift was accommodated by deep-seated thrust faults, such as the Rincón and Toro thrusts (Fosdick et al., 2011) (Fig. 2). This marked a change in structural style during Neogene time from thin-skinned to thick-skinned deformation and reactivation of Mesozoic rifts (Harambour, 2002; Radic et al., 2007). Both the Jurassic rift deposits and the Late Cretaceous Magallanes basin have been intruded by Miocene calc-alkaline to alkaline backarc plutons such as the Torres del Paine and Cerro Fitz Roy granitic massifs (Michael, 1984; Sánchez et al., 2008; Ramírez de Arellano et al., 2012). Lastly, late Cenozoic expansion of the Patagonian ice sheet has strongly modified the physiography of the Patagonian Andes by glaciofluvial processes (Clapperton, 1989; Rabassa, 2008; Lagabrielle et al., 2010; Solari et al., 2012).

3. Methods

Low-temperature (U–Th)/He thermochronology based upon retention of ^{4}He produced during the decay of radioactive ^{238}U, ^{235}U, and ^{232}Th in zircon and apatite can be used to constrain the thermal history of the upper crust (Zeitler et al., 1987; Wolf et al., 1996; Farley, 2002; Reiners et al., 2004). At temperatures above ~200 °C for zircon and ~75 °C for apatite, diffusivities are sufficiently high that effectively all He diffuses from the U- and Th-bearing host. As temperatures decrease when rocks approach the surface, He is progressively retained within the crystal. The temperature range over which this transition occurs is termed the "partial retention zone" (PRZ) and spans ~170–200 °C for zircon (Reiners et al., 2004)

Table 1
(U–Th)/He thermochronology sample locations and information. Refer to Data Repository for single-grain ages.

Sample	Latitude	Longitude	Elevation (m)	No. of grains	Lithostratigraphic interval
ZIRCON					
07-TP2	50°52′11.99039″S	072°40′5.06478″W	1055	4	Coniacian–Maastrichtian sandstone
07-19	51°10′35.06761″S	072°57′48.05606″W	14	3	Cenomanian–Turonian sandstone
07-27	51°07′42.96416″S	072°37′52.67236″W	563	3	Coniacian–Maastrichtian sandstone
07-29	51°07′36.04824″S	072°40′37.88367″W	868	3	Coniacian–Maastrichtian sandstone
07-43	51°17′36.87712″S	072°43′27.58702″W	242	2	Cenomanian–Turonian sandstone
07-56	51°04′32.91957″S	073°14′47.33589″W	186	3	Jurassic rhyolite
07-72	51°03′1.34767″S	073°04′47.20043″W	252	3	Miocene gabbro (17 Ma)
07-84	51°14′33.46481″S	073°01′4.77929″W	110	2	Cenomanian–Turonian sandstone
07-116	51°05′51.63338″S	073°18′27.56007″W	431	4	Aptian sandstone
07-123	51°20′11.31818″S	072°52′59.09468″W	423	3	Jurassic rhyolite
08-135	51°33′43.37841″S	074°04′23.29658″W	1	3	Granodiorite (101 Ma)
08-140	51°18′29.25917″S	073°58′13.65735″W	130	3	Granodiorite (Cretaceous?)
08-143	51°27′1.87598″S	073°33′12.17717″W	75	3	Jurassic metatuff
08-152	51°29′23.27866″S	073°36′16.40527″W	221	3	Granodiorite (80 Ma)
08-153	51°29′51.80582″S	073°35′4.06462″W	268	4	Granophyre (150 Ma)
09-168	51°20′0.73633″S	072°53′4.75056″W	363	4	Jurassic metatuff
09-180	51°22′36.60392″S	072°50′44.97580″W	1309	3	Cenomanian–Turonian sandstone
09-190	51°18′23.39763″S	073°12′53.13926″W	97	4	Cenomanian–Turonian sandstone
09-217	51°19′55.88453″S	072°48′40.77503″W	27	4	Albian volcanic tuff
10-63	51°04′53.08739″S	072°33′39.86414″W	75	2	Coniacian–Maastrichtian sandstone
10-64	51°00′3.96273″S	072°58′50.52222″W	873	3	Miocene granite (TPIC)
10-132	51°26′10.41495″S	073°21′18.71288″W	90	2	Jurassic metatuff
10-133	51°26′47.35618″S	073°20′53.60565″W	84	3	Jurassic metatuff
APATITE					
LF05	51°22′45.25818″S	072°25′44.77123″W	56	4	Coniacian–Maastrichtian sandstone
CCS	51°13′55.62588″S	072°20′41.01598″W	200	3	Coniacian–Maastrichtian sandstone
CM1	50°46′52.31700″S	072°39′47.68329″W	1070	3	Coniacian–Maastrichtian sandstone
CB1	51°20′14.03289″S	072°39′10.04292″W	786	3	Coniacian–Maastrichtian sandstone
F051	50°42′19.42974″S	072°43′29.04692″W	1268	3	Coniacian–Maastrichtian sandstone
07-3	51°09′11.15534″S	073°01′50.41579″W	98	4	Cenomanian–Turonian sandstone
07-4	51°08′45.90444″S	073°01′21.79115″W	210	4	Cenomanian–Turonian sandstone
07-9	51°01′25.21210″S	073°09′26.02789″W	134	3	Cenomanian–Turonian sandstone
07-18	51°07′25.36996″S	073°05′4.55175″W	80	4	Cenomanian–Turonian sandstone
07-19	51°10′35.06761″S	072°57′48.05606″W	14	3	Cenomanian–Turonian sandstone
07-21	51°02′38.00985″S	072°54′52.60337″W	115	4	Coniacian–Maastrichtian sandstone
07-24	51°01′49.34818″S	072°52′5.86311″W	208	3	Coniacian–Maastrichtian sandstone
07-30	51°07′20.30778″S	072°40′32.75692″W	1035	4	Coniacian–Maastrichtian sandstone
07-56	51°04′32.91957″S	073°14′47.33589″W	186	3	Jurassic rhyolite
07-59	51°06′41.51140″S	073°06′54.78768″W	83	3	Cenomanian–Turonian sandstone
07-72	51°03′1.34767″S	073°04′47.20043″W	252	2	Miocene gabbro
09-190	51°18′23.39763″S	073°12′53.13926″W	97	2	Cenomanian–Turonian sandstone
09-217	51°19′55.88453″S	072°48′40.77503″W	27	2	Albian volcanic tuff

and ~55–75 °C for apatite (Wolf et al., 1996; Farley, 2000; Flowers et al., 2009). At lower temperatures, radiogenic He is quantitatively retained.

We have performed (U–Th)/He thermochronology measurements across the Patagonian orogenic belt between latitude 50°30′–51°30′S (Fig. 2). This entailed analysis of 22 zircon samples (74 single grains) and 18 apatite samples (57 single grains) (Table 1). Analytical procedures and single-grain results are described in the Data Repository. Our sampling coverage aimed to constrain exhumation patterns across the major lithotectonic domains shown in Fig. 2; sample collection from the interior of the western thrust domain was hindered by field access and glacial ice cover. As indicated, most of our (U–Th)/He samples are from the retroarc thrust-belt domains, where Mesozoic sedimentary and volcanogenic rocks are variably deformed and low-grade metamorphosed (Figs. 2 and 3). For sedimentary rocks, sampling was restricted to medium-grained sandstones to help ensure that the grain sizes that determine the He diffusive lengths scale and alpha-ejection corrections were comparable to those that characterize the crystalline rocks further west. During the active phases of the thrust-belt, we assume that exhumation inferred from thermochronology ages reflects erosional denudation during faulting. In the absence of documented thrusting, we attribute exhumation to fluvioglacial processes.

4. Results

Weighted mean (U–Th)/He cooling ages were calculated from between two and six single-grain analyses per sample (data repository Tables A-1 and A-2) (Fig. 2). For samples that yield a spread of single-grain ages, such as partially-reset sandstones, we report the range of single-grain ages. Fig. 3 shows the distribution of single-grain (U–Th)/He ages across the Patagonian orogenic belt. In general, zircon (U–Th)/He (ZHe) ages define a regional 'J-shaped' distribution of ages between 15 and 86 Ma with minimum ages centered across the central thrust domain (Figs. 2 and 3). Apatite (U–Th)/He (AHe) ages range from 10 to 4 Ma and are uniform within samples (Table A-2).

4.1. Patagonian batholith

ZHe results from the eastern edge of the Patagonian batholith yield ages between 44 and 20 Ma. The westernmost sample (09-135) is a Late Cretaceous hornblende granodiorite that yields single-grain ages that do not statistically overlap, but together indicate ca. 22–28 Ma ZHe ages. To the north on Isla Evans, sample 09-140 from a Jurassic granodiorite (Hervé et al., 2007a) yields a ZHe age of ca. 44 Ma (Fig. 2). Single-grain ages for this sample range from 39 to 54 Ma; we note a positive correlation

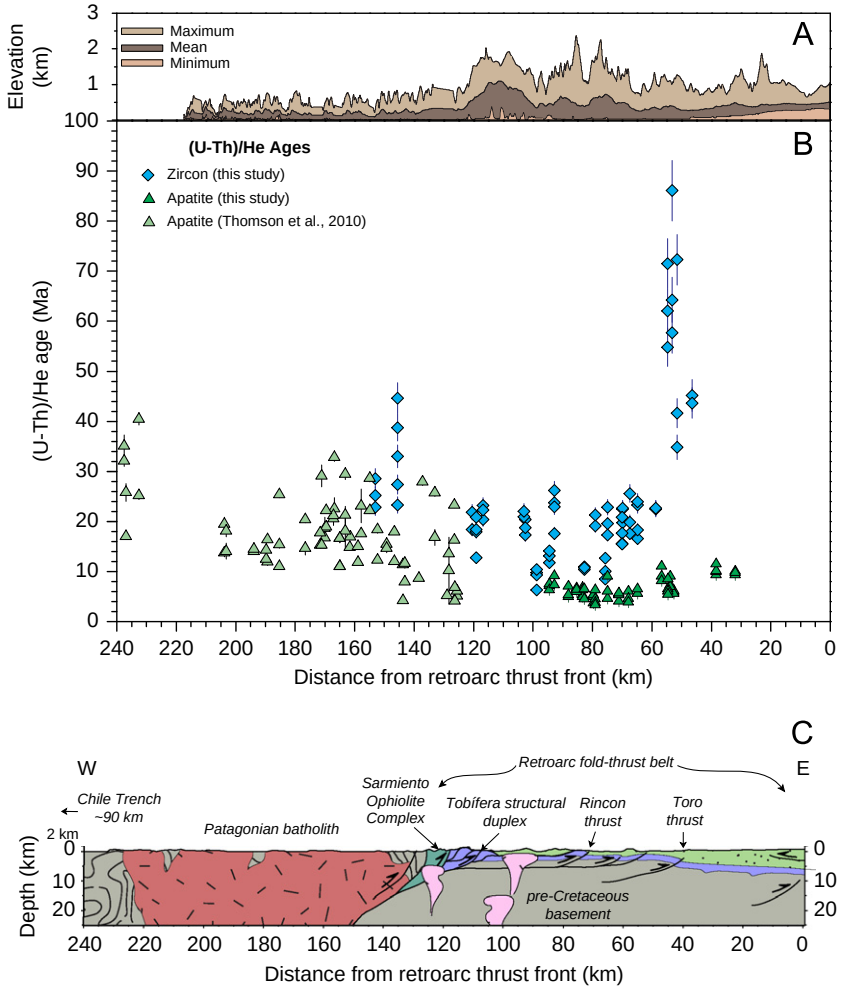

Fig. 3. (A) Elevation across the Patagonian Andes between 50°30′–51°30′S, constructed from swath elevation transects of SRTM 90-m digital elevation model. (B) (U–Th)/He thermochronologic ages from the Patagonian Andes. Zircon ages (blue diamonds) form a pronounced U-shaped pattern with the youngest ages centered on the eastern side of the Andes within the thrust-belt. Apatite ages (dark green triangles) are youngest east of the present-day drainage divide. For comparison, published apatite (U–Th)/He data between 49 and 51°S, compiled from Thomson et al. (2010) (light green triangles), document eastward younging ages on the western side of the drainage divide. (C) Simplified structural cross-section of the Patagonian Andes showing location of major retroarc structures (modified from Fosdick et al. (2011)).

between age and grain-size that may reflect an underestimate of alpha-ejection correction related to zoning in U and Th concentration (e.g., Hourigan et al., 2005) (Table A-1). Farther east, near the western margin of the western thrust domain, results from sample 08-152 (ca. 80 Ma porphyritic granodiorite (Calderón et al., 2012), yield ca. 20 Ma weighted-mean ZHe age.

4.2. Western thrust domain

Upper Jurassic granophyre, metatuff, and hypabyssal rhyolite from the Tobífera structural duplex within the western thrust domain yield a restricted range of single-grain ZHe ages between 24 and 17 Ma (Figs. 2 and 3). Sample 08-143 was collected from a strongly sheared metatuff within the western flank of the duplex and yields a 22.5 Ma weighted-mean ZHe age. Similarly, the eastern side of the Tobífera structural duplex also yields weighted-mean ZHe ages of 21 and 19 Ma (samples 10-132 and 10-133). Sample 07-56 was collected from a rhyolite porphyry along the northeastern edge of the western thrust domain (Fig. 2) and yields ca. 13 Ma and 7 Ma ZHe and AHe ages, respectively. Nearby, the overlying Lower Cretaceous Zapata Formation exposed on the flanks of the Tobífera structural duplex (sample 07-116) yields a 10 Ma ZHe age (Fig. 2).

4.3. Central thrust domain

All samples in the central thrust domain are characterized by similar replicate single-grain ages within each sample, indicative of complete helium degassing of the detrital grains during post-depositional burial (Table A-1). Most ZHe ages from across the southern portion of the central thrust domain are between 22 and 18 Ma. The youngest ZHe ages from the Central thrust domain are located in the northern portion of the study area and range from 13 to 10 Ma (Fig. 2). AHe ages from the central thrust domain range from 8 to 4 Ma (Fig. 3). Most of these samples are from the strongly faulted and folded Cenomanian through Campanian siliciclastic rocks (Wilson, 1991). Late Cenozoic AHe ages from the central thrust belt span ~1200 m of elevation and indicate a subtle positive correlation between age and elevation across the study area (data repository Fig. A-1).

4.4. Eastern thrust domain

(U–Th)/He results from the eastern thrust domain yield relatively older ZHe and AHe ages compared to the central thrust domain (Fig. 2). These samples were collected from Coniacian–Santonian foreland strata exposed in thrust sheets, at stratigraphically high positions in the Cretaceous sedimentary section (Covault et al., 2009; Romans et al., 2011) (Table A-1). ZHe ages show a spread of single-grain ages—most of which are younger than depositional age—that likely reflect burial temperatures to within the PRZ and partial-resetting of detrital ages. Sample JF-07-27 is from a Campanian sandstone and yields ZHe ages between 34 and 72 Ma ($n=3$) (Table A-1). Similarly, sample JF-07-TP2A from a stratigraphically higher level yields 56–314 Ma ZHe ages. For these samples with a range of single-grain detrital ages, we denote then as PRZ symbols in Fig. 2. The oldest AHe

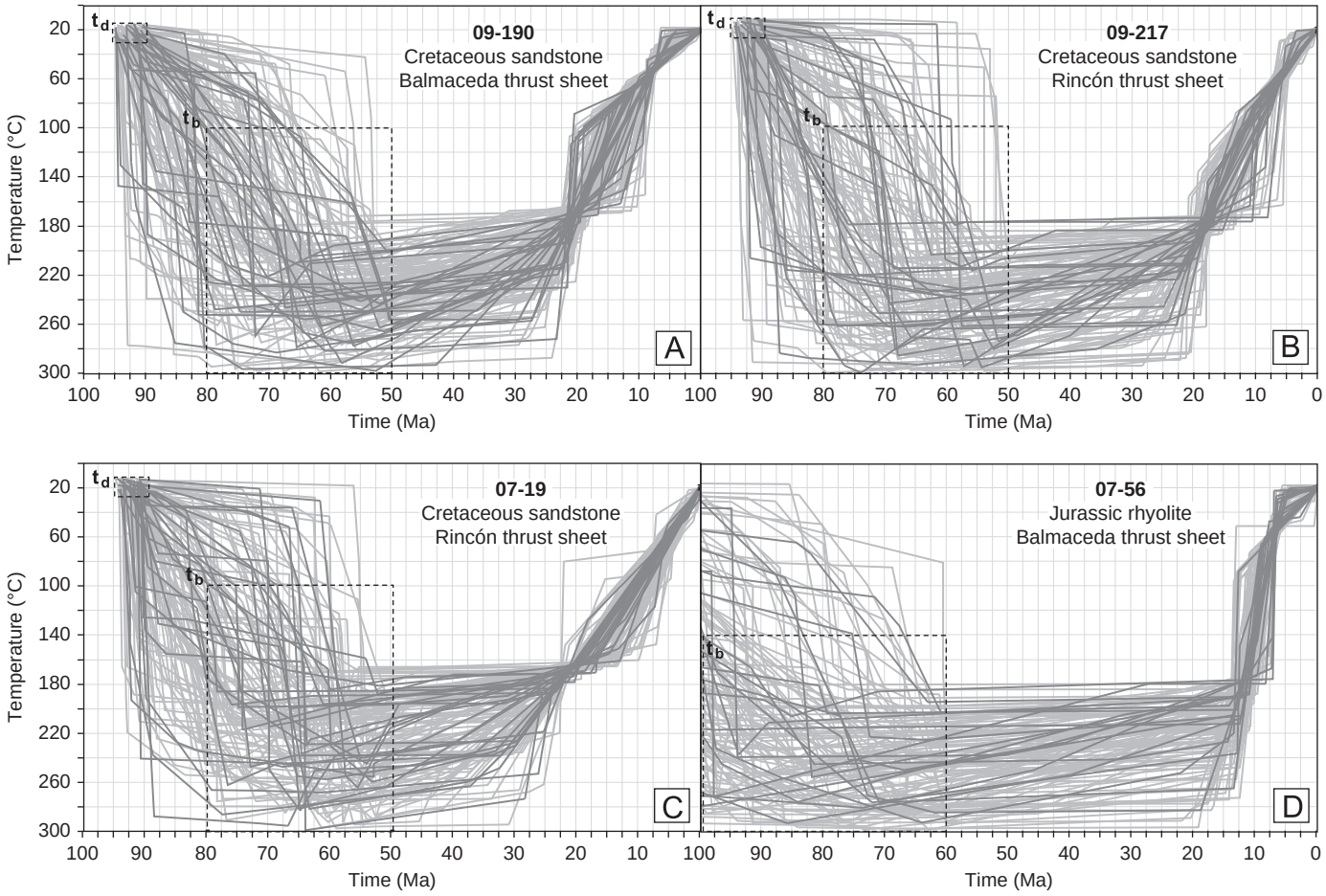

Fig. 4. Time–temperature model results for selected samples using HeFTy (Ketcham, 2005). *T–t* envelopes represent thermal paths with acceptable goodness of fit (GOF) > 0.5 (light gray) and good GOF > 0.05 (dark gray). Black dashed boxes indicate additional constraints based on the depositional age (t_d) and range of plausible post-depositional burial heating history (t_b).

ages (10–8 Ma) in this study are recorded in the easternmost Campanian–Maastrichtian foreland basin deposits exposed along the frontal monocline of the Patagonian fold-thrust belt (Fig. 2). Single-grain replicate AHe ages for these samples show excellent reproducibility and indicate complete post-depositional helium degassing of the foreland succession prior to Cenozoic cooling (Table A-2).

4.5. Inverse thermal modeling

We modeled the time–temperature histories of four samples from the thrust-belt using a Monte-Carlo inversion algorithm of HeFTy® (Ketcham, 2005) in order to evaluate the magnitude and timing of thrust-belt cooling in relationship to geologic events in Patagonia. In addition to the ZHe and AHe data, the ranges of possible thermal histories are constrained by sample depositional age (t_d) and a wide temperature window of foreland burial temperatures (t_b) during foreland burial prior to unroofing (Fig. 4). Model results for the Mesozoic sedimentary rocks represent post-depositional burial during Paleogene time, consistent with complete outgassing of detrital zircon and apatite (U–Th)/He ages. For the southern samples (Fig. 4A–C), self-consistent thermal paths from ca. 22 to 0 Ma suggest uniform cooling from temperatures above 180 °C. By contrast, model results from rocks located near the Torres del Paine intrusion require a younger closure through ZHe PAZ ca. ~12–11 Ma (Fig. 4D), which we attribute to local magmatic heating (discussed below).

5. Discussion

Interactions between tectonic and surface processes exert complex and evolving relationships between the distribution of deformation within the thrust wedge, morphology (width, elevation, drainage organization), and long-term erosional processes. We examine the Cenozoic exhumational record across the Patagonian Andes within the regional tectonic, depositional, and climatic context of its position along the southern end of a major orogenic belt. Of particular importance to consider throughout the discussion are the first-order physiographic changes along the South America continent, whose width narrows southward by a factor of nearly three, crustal thickness decreases from ~40–80 km in the central Andes (Zandt et al., 1994; Yuan et al., 2006; Fromm et al., 2004) to ~28–36 km across Patagonia (Robertson Maurice et al., 2003; Lawrence and Wiens, 2004), and high topography decreases southward. South of ~32°S, the Patagonian retroforeland resides in a modern-day orographic rainshadow in the lee of the high Cordillera. Additionally, the foreland basin record along southern Patagonia reflects its extensive Mesozoic backarc rift-basin history and predominantly deep-marine foreland depositional systems (e.g., Fildani et al., 2008) compared to the mostly continental sedimentation within foreland basin depocenters in the central Andes (e.g., Horton, 1999). Finally, the southern edge of the South American continent is subject to oblique plate interactions with the Scotia and Antarctic plates, giving rise to complex plate boundary stress configurations during the Cenozoic evolution of the orogenic belt (e.g., Barker, 2001; Lagabrielle et al., 2009; Barbeau et al., 2009).

5.1. Exhumation patterns across the Patagonian Andes

Our thermochronology results suggest that the Patagonian retroarc thrust-belt has undergone significant foreland burial and subsequent exhumation characterized by spatio-temporal variations in Cenozoic time. (U–Th)/He ages determined from crystalline basement rocks are generally interpreted in terms of regional cooling as bedrock approaches the surface in response to

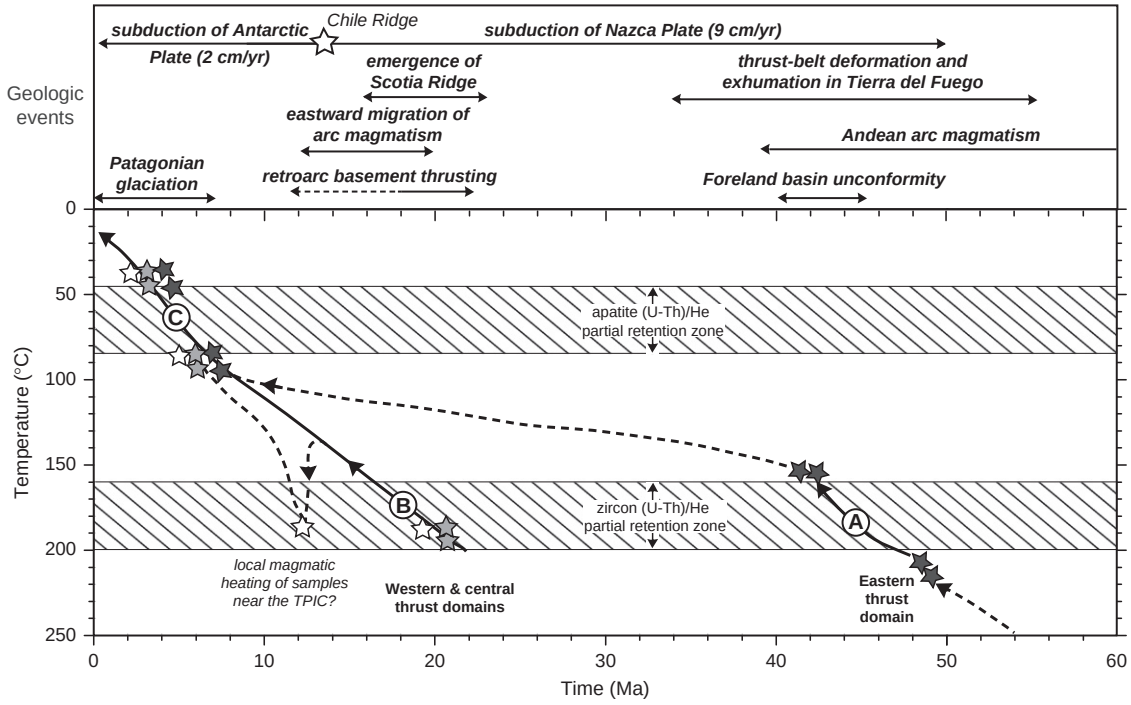

Fig. 5. Cenozoic thermal history of the Patagonian thrust-belt domains in comparison to regional geologic events in Patagonia: (A) thrust sheets in the eastern thrust domain (dark gray stars) record protracted Paleogene cooling through zircon PRZ. (B) Farther west, rocks in the western and central thrust domain (light gray and white stars) are interpreted to record regional exhumation through the zircon PRZ between 22 and 18 Ma, synchronous with onset of retroarc basement thrusting. Local magmatism ca. 12 Ma may have partially-reset nearby samples (white star). (C) Nearly all samples from the Patagonian retroarc region record erosion-driven cooling through the apatite PRZ between 7 and 4 Ma. Solid segments of schematic cooling paths indicate T–t paths well-constrained by thermochronology data and thermal modeling and dashed segments denote increased ambiguity. Refer to text for discussion and references for geologic events.

erosion or tectonic processes (Ehlers, 2005). In the case of sedimentary or volcanic rocks of the thrust-belt, the situation is more complicated because detrital zircon and apatite retain radiogenic He when burial temperatures were within or below the PRZ. This ambiguity applies to the Patagonian Andes where Upper Jurassic–Cretaceous sedimentary rocks within the thrust-belt exhibit spatially variable partial-to complete-resetting of detrital zircons and complete resetting of detrital apatite (Tables A-1 and A-2).

Below we discuss the thermal history of the Patagonian thrust-belt in relation to major tectonic and climatic events shown in Fig. 5. The spatially uniform distribution of invariant single-grain ZHe ages ca. 22–18 Ma from across Patagonian Cordillera and the central thrust domains indicate that burial temperatures achieved during thrusting exceeded ~180 °C (white and light grey stars in Fig. 5). Numerical modeling results of the ZHe and AHe ages for samples from the central thrust domain reveal rapid cooling through the zircon PRZ beginning ca. 22 Ma (Fig. 4). Such elevated temperatures are consistent with the observed regional sub-greenschist facies metamorphism that occurred during tectonic burial of the Upper Cretaceous basin-fill (Fildani and Hessler, 2005). The observation that ZHe ages are invariant across both the western and central thrust domains (Fig. 3) requires that the Tobífera duplex and hanging walls of the Rincón and Toro thrust faults resided at crustal temperatures greater than the ZHe PRZ prior to rapid cooling 22–18 Ma (Figs. 4 and 5).

Toward the foreland, within the eastern thrust domain, the older ZHe ages, with larger spread of partially-reset single-grain ages, (Fig. 3) yield evidence for Paleogene thrust burial and Eocene exhumation. One sample yields invariant single-grain ages ca. 44–43 Ma, while stratigraphically higher samples yield a range of ages, the youngest of which are ~35–44 Ma (Table 1). Since no single-grain ages from these samples are younger than latest Eocene–early Oligocene, we use 35 Ma as a nominal constraint for when these strata cooled below the ZHe PRZ. This interpretation is validated by detrital thermochronology data from the Cenozoic basin record, where post-depositional heating of the overlying Paleocene deposits likely ceased by ca. 40–30 Ma (Fosdick, 2012). The Paleogene deformational record at this latitude in the Andes is obscured by sparse temporal constraints on faulting, leading to reliance on data from Tierra del Fuego, where structural and geo-thermochronologic studies report Paleogene internal deformation, structural uplift, and exhumation (Klepeis, 1994; Kohn et al., 1995; Kraemer, 2003; Klepeis et al., 2010). Because much of the Paleogene sedimentary record is missing in our study area, many workers have interpreted that erosional denudation occurred during the Paleogene and that this coincided with eastward migration in basin depocenter (e.g., Biddle et al., 1986; Malumián et al., 2000; Fosdick et al., 2011). We accordingly interpret the Paleogene ZHe ages as recording cooling in response to thrusting-induced erosional denudation at this time (Fig. 5).

Interpretation of retroarc exhumation is more complicated for some of the younger (12–10 Ma) ZHe samples in the northern part of the central thrust domain, located near the ca. 12.5 Ma Torres del Paine Intrusive Complex (TPIC; Michel et al., 2008). Transient heating related to Torres del Paine magmatism may account for the younger (12–10 Ma) ZHe ages compared to those

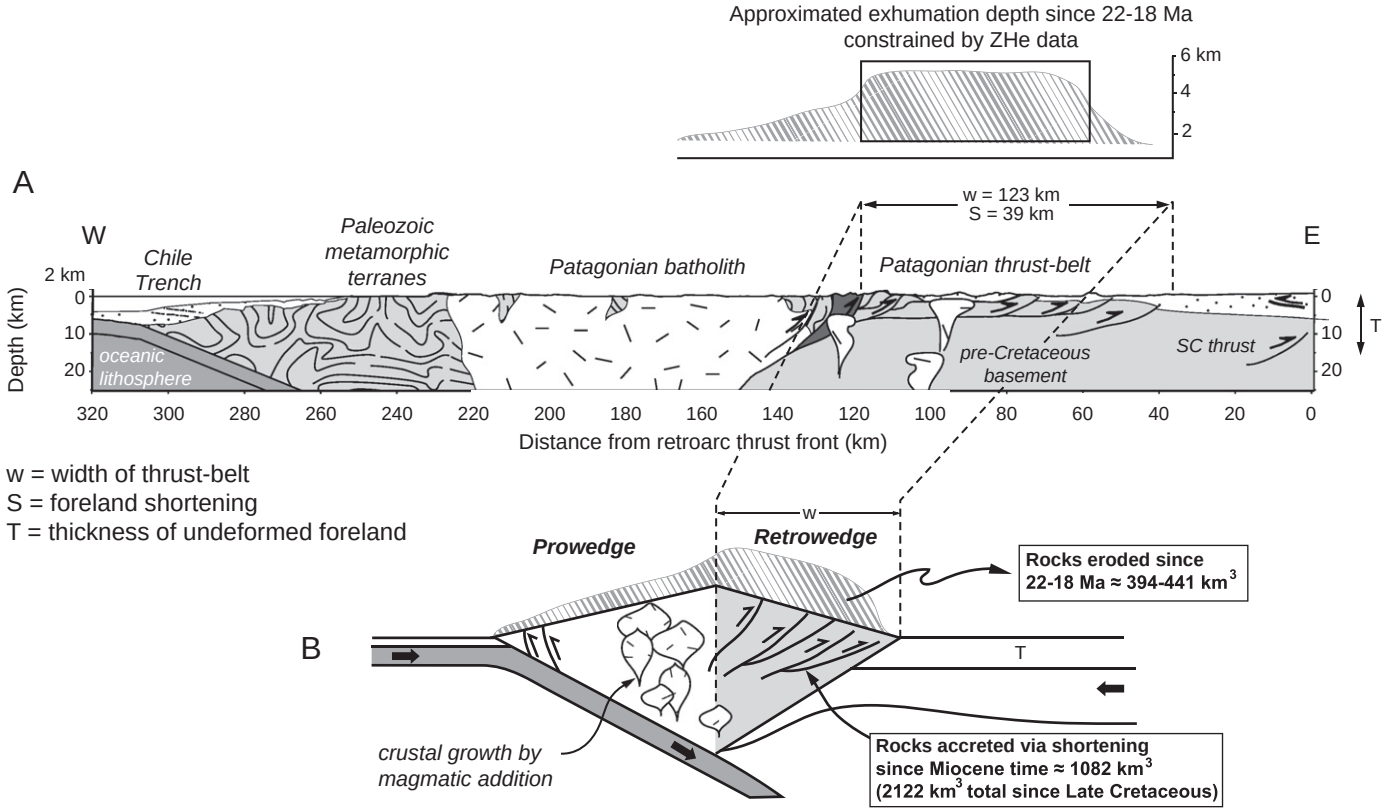

Fig. 6. Comparison between structural development of the Patagonian fold-thrust belt and long-term exhumational record since early Miocene time. (A) Simplified cross-section of the Patagonian orogenic wedge showing width of thrust belt (w), depth of foreland decollément (T), and minimum shortening (S) (after Fosdick et al. (2011) and references therein). (B) Schematic illustration of doubly-vergent wedge (not to scale) showing estimated cross-sectional area of rocks removed from the thrust belt since 22–18 Ma, calculated from zircon (U–Th)/He ages. Includes conceptual aspects of Sanders et al. (1999), DeCelles and DeCelles (2001), and McQuarrie et al. (2008).

collected further south (Fig. 5). The TPIC laccolith is thin (<1 km), with a shallow emplacement depth of 2–3 km (Putlitz et al., 2001) and thus a probably limited source of magmatic heat. However, it is possible that latent heat liberated from Miocene pluton rock at greater depth could have elevated the local thermal gradient, thereby accounting for the 12–10 Ma ZHe ages from nearby bedrock samples (Fig. 5).

While the hinterland of the thrust-belt including the Patagonian Batholith have undergone the deepest levels of exhumation within the overall Andean orogenic belt at latitude 51°S, the timing of this exhumation is older than that exhibited by the thrust-belt. Thermobarometry of Late Jurassic plutons along eastern edge of the batholith (Fig. 2) suggest crystallization occurred at >20 km depth (Massonne et al., 2004). Further east in the western thrust domain, the Tobífera Formation also records comparably deep levels of exposure (16–22 km), based on syntectonic upper greenschist facies metamorphic mineral assemblages (5–7 kb; 230–350 °C) (Hervé et al., 2007b; Calderón et al., 2012). Calderón et al. (2012) report that these rocks cooled below the phengite $^{40}Ar/^{39}Ar$ retention zone (400–300 °C) between ca. 85 and 80 Ma.

Our early to middle Miocene ZHe ages across the orogen generally agree with a regionally observed eastward migration of denudation documented within the forearc region (Thomson, 2002; Thomson et al., 2001) (Fig. 3). The batholith was exhumed through apatite fission-track closure temperatures (110–60 °C) starting in Paleocene time in the west, followed by eastward-younging cooling until 12–8 Ma at the present-day topographic divide (Fig. 3) (Thomson et al., 2001, 2010). Our study extends this pattern east of the drainage divide with ZHe and AHe sample coverage of the retroarc region. Young (<10 Ma) AHe ages on the retroarc thrust-belt demonstrate that late Cenozoic denudation was concentrated on the eastern side of the Patagonian Andes (Fig. 3).

5.2. Rates of retroarc exhumation and orogenic mass balance

In order to evaluate temporal changes in exhumation rate within the thrust-belt domains, we compare the HeFTy modeling results with a simple calculation of time-averaged exhumation rates from samples with both ZHe and AHe ages. In the simplest case, this method requires an assumption of a constant geothermal gradient as well as the bulk closure temperature for each thermochronometer. For the Patagonian retroarc region, with high heat flow (~ 75 mW/m^2 after Hamza and Muñoz (1996)) associated with a Cenozoic history of asthenospheric slab window formation, we use a geothermal gradient of 30 °C km^{-1}. Nominal closure depths are inferred between $\sim 60°$ and ~ 180 °C bulk closure temperatures for apatite and zircon crystals, respectively, using 60 μm effective radius, 10 °C surface temperature, and 10 °C km^{-1} uniform cooling rate (Farley, 2000; Reiners et al., 2004) (data repository Table C-1). For all three samples collected from the central thrust domain (samples 07-19, 09-190, and 09-217), we calculate ~ 5–6 km exhumation depth and long-term exhumation rates of ~ 0.22–0.35 mm yr^{-1} since ca. 22 Ma. These nominal estimates are consistent with the cooling paths derived from the HeFTy numerical modeling (Fig. 4A–C).

The long-term morphologic behavior of the Patagonian thrust-belt is considered here by comparing the structural development of the thrust-belt and its exhumational record, based on the premise that the orogen size is modulated by accretionary and erosional fluxes (e.g., Dahlen and Suppe, 1988; DeCelles and DeCelles, 2001; Whipple and Meade, 2006; McQuarrie et al., 2008) (Fig. 6). First, we estimate the magnitude of erosion from the western and central thrust domains (a distance of ~ 75 km), across which nearly all ZHe ages fall between 22 and 18 Ma (Fig. 6). Using a ~ 5.3–5.9 km closure depth calculated from the thermal parameters described above (Table C-3), we estimate ~ 394–441 km^3 per strike length of upper crustal rocks have been eroded since early Miocene time (Fig. 6).

By contrast, we approximate a minimum of ~ 2122 km^3 per strike length of rocks accreted to the orogenic wedge (e.g., DeCelles and DeCelles, 2001; McQuarrie et al., 2008). This value is the sum of 478 km^3 of rock accreted via shortening since Late Cretaceous time and 1644 km^3 of rock accreted by wedge propagation (Fig. 6) along an 8–12 km deep decollément (Harambour, 2002; Fosdick et al., 2011). We note that most of this accretion occurred during Late Cretaceous and Paleogene stages of deformation, whereas early Miocene and younger accretion accounts for ~ 1082 km^3 (Fosdick et al., 2011). These mass flux calculations demonstrate that erosional processes have removed ~ 36–40% of the accretionary volume over the past 22 Myr, leaving relatively less mass to build topography in the thrust-belt since early Miocene time (Fig. 6). Most erosion has occurred within the interior of the thrust-belt (the western and central thrust domains), whereas the final stage of mass accretion (ca. 22–10 Ma) was accommodated by thrust propagation and wedge-widening with relatively less shortening.

5.3. Synchronous deformation, retroarc exhumation, and sedimentation

Overall, we interpret ZHe data from the Patagonian Andes to reflect synchronous regional exhumation across the orogen between 22 and 18 Ma, focused on the Tobífera structural duplex and Upper Cretaceous strata in the central thrust domain (Fig. 3). In the retroforeland, thrust faults that are seated in pre-Jurassic basement have uplifted the thin-skinned thrust-belt by ~ 5 km above regional basement depths (Fig. 3). Seismic-reflection data and geologic mapping characterize several 30–35° west-dipping faults that flatten into a decollément at 8 km depth, thereby passively folding older thin-skinned faults across regional hanging-wall anticlinal structures (Harambour, 2002; Fosdick et al., 2011). Although available subsurface data do not extend far west beneath the central thrust domain, this basement geometry, coupled with the presence of Upper Jurassic rocks exposed in the Rincón thrust sheet, suggest structural uplift and associated unroofing along similar structures.

Early Miocene regional exhumation of the central thrust domain coincides with a phase of foreland deformation along the Toro thrust (Fig. 2) and activation of a deeper basal decollément ca. 22 Ma (Fosdick et al., 2011). Limited geologic data are available to constrain the timing of Toro faulting. Open folding of the Upper Cretaceous stratigraphic section within the hanging-wall of the Toro thrust occurred after intrusion of a 21 Ma gabbroic sill and during 22–18 Ma synorogenic foreland sedimentation (Fosdick et al., 2011). We interpret our ZHe data and modeling results (Fig. 4) to reflect thrust-related unroofing across the Toro thrust and out-of-sequence thrusting along the Rincón thrust and possibly other basement structures beneath the central thrust domain (Fig. 2). Finally, we note that coeval 22–18 Ma ZHe ages exhumation ages also occur further west across the western thrust domain, where the Late Cretaceous (~ 85 Ma) sub-vertical Canal de las Montañas shear zone (CMSZ) accommodates east-directed thrusting within the Sarmiento ophiolitic complex and Tobífera duplex (Calderón et al., 2012). Paleomagnetic data indicate $\sim 30°$ of westward horizontal-axis rotation of the ophiolitic complex along deep-seated structures such as the CMSZ (Rapalini et al., 2008). Early Miocene exhumation inferred from our ZHe results may in fact be associated with this out-of-sequence deformation.

The sedimentary record from the Magallanes foreland basin is consistent with an early Miocene increase in erosion rates across the thrust belt, reflected by an increased sediment flux from the Oligocene/early Miocene shallow-marine Centinela Formation to the high-energy fluvial–alluvial early-middle Miocene Santa Cruz Formation (Malumián and Caramés, 1997; Blisniuk et al., 2005; Parras et al., 2008). Previous workers have interpreted the Santa Cruz Formation as synorogenic fill associated with the main phase of Andean uplift (Ramos, 1989, 2005) between 22 and 14 Ma (Blisniuk et al., 2005). In the thrust-belt, our ZHe results demonstrate regional denudation coeval with continental foreland sedimentation (Fig. 5).

We propose that the synchronicity of early Miocene thrust-belt deformation, exhumation, and foreland sedimentation events in the retroarc region occurred in response to a tectonic plate reorganization at the southern end of South America and opening of the Scotia Sea ca. 23–20 Ma (Cunningham et al., 1995; Barker, 2001; Lagabrielle et al., 2009) (Fig. 5). Since Oligocene time, transpressional deformation and associated wrench tectonics have strongly modified the shape of the tip of the continent (Ghiglione and Ramos, 2005). Between 23 and 20 Ma, growth of the submerged North Scotia Ridge and Tierra del Fuego, orthogonal to the Patagonian thrust-belt (Cunningham et al., 1995; Barker, 2001; Eagles et al., 2005) (Fig. 1), could have transmitted stresses westward into the Patagonian foreland (Lagabrielle et al., 2009). In this view, regional stress configurations promoted deep-seated thrusting, rock uplift, and unroofing of the Patagonian thrust-belt in early Miocene time (Fig. 5). These events ca. 23–20 Ma could also be more broadly linked to a change in tectonic plate motion from oblique to orthogonal convergence between the Nazca and South American plates beginning ca. 26 Ma (Cande and Leslie, 1986; Pardo-Casas and Molnar, 1987). Sustained early-middle Miocene erosion of the growing thrust-belt would have provided ample sediment to east-flowing river systems, such as the Santa Cruz Formation, and prograding subaqueous deltas into the Atlantic Ocean.

Some workers have proposed a causal relationship between retroarc contractional deformation and collision of the Chile Ridge, an oceanic spreading center obliquely subducting beneath the South American margin (Suárez et al., 2000; Ramos, 2005; Lagabrielle et al., 2010). Plate reconstructions and backarc magmatism signal the subduction of the Chile at the latitude of our study area ca. 14–13 Ma (Cande and Leslie, 1986; Ramos and Kay, 1992; Gorring et al., 1997; Ramos, 2005; Breitsprecher and Thorkelson, 2009) (Fig. 5). Our thermochronology ages do not directly coincide with the timing of the Chile Ridge collision at 14–13 Ma (Gorring et al., 1997) (Fig. 5). Rather, the ZHe ages are significantly older and thermal modeling results are consistent with cooling beginning as early as ca. 22 Ma (Fig. 4). For the lower-temperature chronometer, AHe ages (8–4 Ma) post-date ridge subduction and appear to be more closely timed with late Cenozoic changes in climate and erosional regime (Fig. 5). However, we also consider the possibility that the older AHe ages (10–8 Ma) could reflect delayed response (e.g., Guenthner et al., 2010) to reheating of the overlying lithosphere following ridge–trench collision.

5.4. *Late Cenozoic fluvioglacial erosion of the Patagonia retroarc region*

Late Cenozoic glaciation and exhumation history of the Patagonian orogen bears on our interpretation of the apatite (U–Th)/He results, which are particularly sensitive to surface processes and changes in erosion rate. Lagabrielle et al. (2010) summarize the Mio-Pliocene glacial record of Patagonia, which includes evidence for glacial processes as early as 7 Ma in the north (Mercer and Sutter, 1982; Ton-That et al., 1999) and 10 Ma near 49°S (Wenzens, 2006). These glacial archives are consistent with increased sedimentation rates at ca. 7 Ma documented in the Chile trench (e.g., Bangs and Cande, 1997; Melnick and Echtler, 2006), in addition to higher erosion rates along the Patagonian Andes since ca. 10 Ma (Thomson et al., 2010).

Our AHe age results from the Patagonian retroarc region appear to document coeval erosional denudation related to glaciation between 8 and 4 Ma (Fig. 5). While foreland shortening and associated thrust-driven exhumation may be as young as ~14–10 Ma along the eastern edge of the thrust-belt (Fosdick

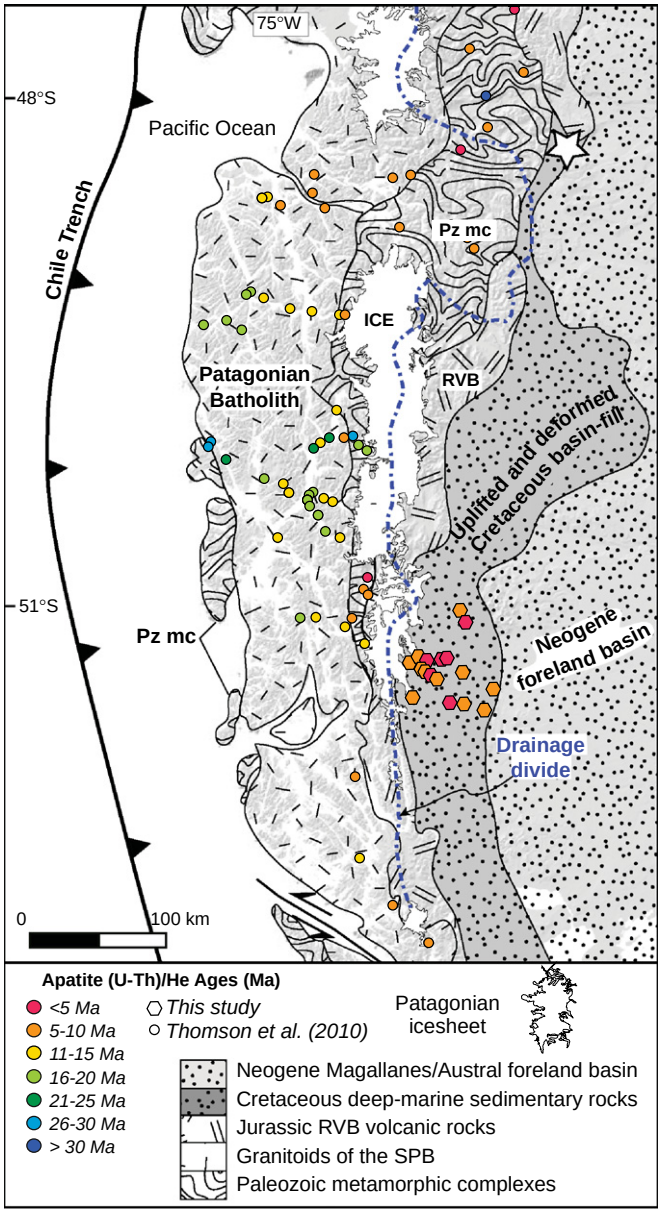

Fig. 7. Simplified lithotectonic domains of the Patagonian Andes with apatite (U–Th)/He ages from this study (hexagons) and those plotted from Thomson et al. (2010) (circles). West of the present-day drainage divide, ages depict an eastward younging pattern of Cenozoic exhumation. South of 49°30′S, the fine-grained siliciclastic basin fill of the Upper Cretaceous Magallanes Basin is exposed in the retroarc thrust belt. In contrast, the retroarc region north of this latitude constitutes mostly metamorphic and volcanic rocks. White star shows position of the Blisniuk et al. (2005) paleoaltimetry study discussed in the text. Regional geology after SERNAGEOMIN (2003) and SEGEMAR (1997). RVB—Rocas Verdes Basin; SPB—Southern Patagonian Batholith; PZ mc—Paleozoic metamorphic complex.

et al., 2011), the paucity of late Mio-Pliocene or younger structures in the central thrust-belt argues against a tectonic driver for the late Mio-Pliocene erosion at this latitude. Instead, erosional bedrock glacial troughs, areal scouring, and extensive glacial striations are common features in the western and central thrust domains, suggesting major modification to the landscape by glacial processes (Solari et al., 2012). Geomorphic and structural studies in the Lago Argentino area to the north demonstrate an important transition of a broad, low-relief landscape that becomes deeply incised by glacial valleys ca. 3 Ma (Lagabrielle et al., 2010; Scalabrino et al., 2011). In our study area, some of our youngest AHe ages may reflect similar coeval glacial-incision of the thrust-belt.

5.5. Comparison of along-strike interactions among exhumation, lithology, and climate

Late Cenozoic erosional denudation is well-documented in the Patagonian Andes by regional thermochronology along the length of the orogen. We note that these regional datasets are largely representative of the windward (prowedge) side of the Patagonian orogen, particularly south of 49°S (Thomson, 2002; Thomson et al., 2001, 2010) (Fig. 7). Published thermochronology datasets characterize older (>10 Ma) AHe ages south of 49°S, compared to younger (<10 Ma) AHe ages located north of this latitude (Thomson et al., 2010). These general spatial patterns in denudation led Thomson et al. (2010) to propose a poleward decrease in the efficiency of late Cenozoic glacial erosion, suggesting that colder-based glaciers in the south are likely to shield the landscape against erosional denudation, compared to their wet-based and highly erosive counterparts in the north. In contrast, our AHe results from the leeward side of the Patagonian orogen record young ages (<10 Ma) centered between 6 and 4 Ma. We interpret these young AHe ages to indicate significant late Miocene and Pliocene denudation, consistent with efficient fluvioglacial erosion across the thrust-belt that has been focused on the *retrowedge* rather than prowedge region (Fig. 7).

Since erosion intensity is related to both long-term global climate patterns and physical properties of the rocks exposed at the surface, we suggest that focused retroarc exhumation in Patagonia may reflect a fundamental change in lithology and physiographic structure towards the southern terminus of the orogenic belt (Fig. 7). The northern Patagonian thrust-belt near Lago Posadas, ~400 km north of our study area, exposes erosion-resistant Paleozoic and Mesozoic metamorphic basement and large thrust-sheets of resistant Jurassic volcanic rocks (Fig. 7) (Suárez, 1976; Ramos et al., 1982; Ramos, 1989). At this altitude, stable isotope and sedimentology data from the foreland basin record surface uplift and aridification ca. 16.5 Ma (Blisniuk et al., 2005), broadly coeval with timing of Miocene deformation observed in the south. Southward, however, the thrust-front progressively uplifts the fine-grained Magallanes basinal rocks

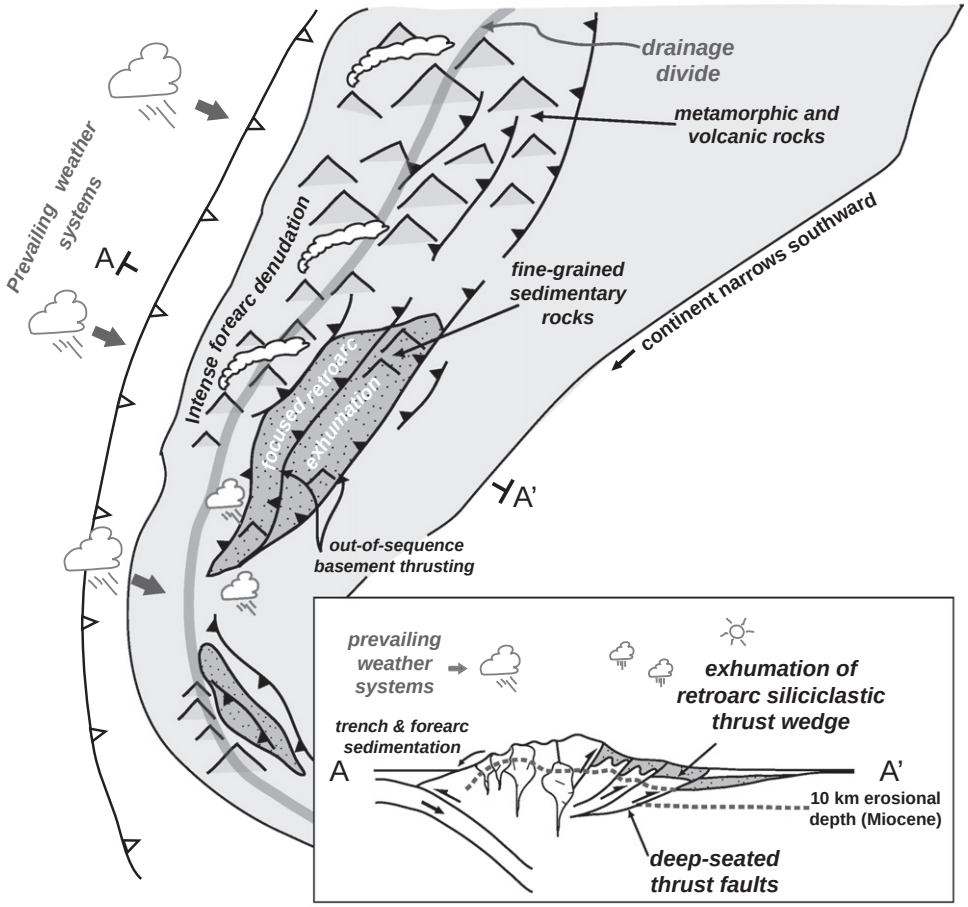

Fig. 8. Schematic model of orogenic exhumation at the narrow end of an orogenic belt, showing effects of inherited basin paleogeography and surface exposure of easily eroded sedimentary rocks. In the north, the thrust-belt consists of resistant metamorphic, volcanic, and coarse-grained clastic rocks and forms an orographic barrier for westerly weather systems. In contrast, the orogenic belt narrows southward, where fine-grained strata are exposed in the hanging walls of out-of-sequence, deep-seated thrust faults (analogous to our study area). Here, additional westerly precipitation may reach the retroarc region as topography decreases southward. Note the higher levels of Miocene crustal exhumation in retroarc region, as depicted by the ~10 km erosional depth (gray-dashed line) in cross-section A–A′.

that are more susceptible to erosion than their crystalline and coarse-grained counterparts to the north (Fig. 7) (Stock and Montgomery, 1999; Sobel and Strecker, 2003; Hilley and Strecker, 2004). In a recent synthesis, Hilley and Coutand (2010) demonstrated that the surface exposure of different rock types, and thus paleogeography, is strongly spatially correlated to variations in long-term orogenic erosion rates. Given the paleogeographic extent of the southward-deepening, fine-grained Magallanes foreland basin in southern South America (Katz, 1963; Suárez, 1976; Biddle et al., 1986; Wilson, 1991), we consider these factors as a geologic explanation for enhanced erosion intensity in the Patagonian retroarc (Fig. 8). It follows that widespread structural uplift of the Cretaceous foreland depocenter since ca. 22–18 Ma could account for extensive exposure of easily eroded rocks, thereby accentuating late Cenozoic exhumation signals in the retroarc region (Fig. 8).

Sustained retroarc denudation in the southern Patagonian Andes may be further explained by southward-deterioration of high topography south of 47°30′S (Fig. 8), a configuration that could allow for the precipitation gradient to broaden southward (Fig. 8). Modern precipitation records reveal that, superimposed on the orographic gradient across the Patagonian Andes, localized zones of high rainfall extend eastward across the mountain belt as well (Legates and Willmott, 1990) (Fig. 1). Furthermore, present-day deciduous ecotones south of 51°S extend farther east than they do in the northern sector (Moore, 1983; Hinojosa and Villagran, 1997), and leeward ice accumulation areas still receive much of the moisture from westerly precipitation (Glasser and Jansson, 2005). Finally, mammal faunal assemblages suggest that wet and forested habitats extended to the tip of the continent during Oligocene–middle Miocene time (Pascual and Ortiz Juareguizar, 1990). While speculative, these emerging denudation patterns motivate additional study of changes in climate, topography, and exhumation along southern Patagonia.

6. Conclusions

In summary, thermochronology data from the southern Patagonian Andes document regional exhumation across the retroforeland thrust-belt from ~5 to 6 km depth belt since 22–18 Ma. Along the eastern thrust domain, ZHe ages between 44 and 42 Ma allude to an episode of Paleogene exhumation along the eastern thrust domain, offering constraints on the nature of the regionally developed foreland unconformity at this time. Although the greatest overall denudation occurred in the Patagonia batholith, our data suggest that exhumation shifted east by the Neogene and has been concentrated in the retroarc region. This episode of thrust-belt exhumation coincided with a deepening of the structural decollément beneath the thrust-belt and likely reflects a retroarc manifestation of plate reconfigurations at the tip of South America and middle Miocene transpressional emergence of the North Scotia Ridge. We conclude that more recent denudation characterized by young AHe ages post-dated deformation and was primarily related to late Cenozoic fluvioglacial erosion, accounting for ~2 km of retroarc denudation since 10–4 Ma.

We propose that enhanced exhumation of the Patagonian Andes since early Miocene time was the combined result of widespread retroarc rock uplift (via deep-seated faulting) that brought easily erodible rocks to the surface and subjected them to erosional denudation (Fig. 8). We further suggest that retroarc denudation at this latitude of the orogen—downwind of an orographic barrier—was enhanced by widespread uplift and unroofing of the fine-grained siliciclastic rocks of the marine Cretaceous foreland basin ca. 22–18 Ma. More speculatively, its position at the narrow, southern end of the Andean orogenic belt may also facilitate access to additional moisture to the retroarc and increase late Cenozoic erosional denudation. These observations suggest that exhumation patterns at narrow terminations of orogens are likely to significantly deviate from the predictions of Andean-type models of orogenic deformation and erosion that feature a strong continental backstop, resistant lithology, and two-dimensional orographic gradients.

Acknowledgments

We thank S. Graham, G. Hilley, T. Dumitru, L. Cruz, M. Brandon, S. Thomson and J. Covault, for invigorating discussions about this work. L. Stright, A. Airo, Z. Jobe, A. Bernhardt, D. Armitage, K. Gillingham, and the Yacht Morgane crew provided excellent field assistance. M. Coble, S. Johnstone, and G. Zhuang assisted with analytical work. We thank S. Hubbard and B. Romans for a few apatite separates. Land access was graciously granted by the Parque Nacional del Torres del Paine and Don Luis Guerrero. This study was supported by the Stanford Project on Deep-water Depositional Systems, funds to S. Graham from the Stanford School of Earth Sciences, American Alpine Club, and Anillo Antártico Project ACT-105. We kindly acknowledge J. Barnes, B. Horton, and an anonymous reviewer for insightful and constructive reviews that greatly improved the scope of this paper.

Appendix A. Supporting information

Supplementary data associated with this article can be found in the online version at http://dx.doi.org/10.1016/j.epsl.2012.12.007. These data include Google map of the most important areas described in this article.

References

Allen, R.B., 1982. Geología de la Cordillera Sarmiento, Andes Patagónicos, entre los 50° 00′ y 52° 15′ Lat. S, Magallanes, Chile. Serv. Nac. Geol. Min. Chile Bol. 38, 1–46.

Bangs, N.L., Cande, S.C., 1997. Episodic development of a convergent margin inferred from structures and processes along the southern Chile margin. Tectonics 16, 489.

Barbeau, D.L., Olivero, E.B., Swanson-Hysell, N.L., Zahid, K.M., Murray, K.E., Gehrels, G.E., 2009. Detrital-zircon geochronology of the eastern Magallanes foreland basin: implications for Eocene kinematics of the northern Scotia Arc and Drake Passage. Earth Planet. Sci. Lett. 284, 489–503.

Barker, P.F., 2001. Scotia Sea regional tectonic evolution: implications for mantle flow and palaeocirculation. Earth-Sci. Rev. 55, 1–39.

Barnes, J.B., Ehlers, T.A., McQuarrie, N., O'Sullivan, P.B., Tawackoli, S., 2008. Thermochronometer record of central Andean Plateau growth, Bolivia (19.5°S). Tectonics 27, TC3003, http://dx.doi.org/10.1029/2007TC002174.

Barnes, J.B., Ehlers, T.A., Insel, N., McQuarrie, N., Poulsen, C.J., 2012. Linking orography, climate, and exhumation across the central Andes. Geology 40, 1135–1138.

Beaumont, C., Fullsack, P., Hamilton, J., 1992. Erosional control of active compressional orogens. In: McClay, K.R. (Ed.), Thrust Tectonics. Chapman & Hall, London, UK, pp. 1–18.

Berger, A.L., Spotila, J.a., Chapman, J.B., Pavlis, T.L., Enkelmann, E., Ruppert, N.a., Buscher, J.T., 2008. Architecture, kinematics, and exhumation of a convergent orogenic wedge: a thermochronological investigation of tectonic–climatic interactions within the central St. Elias orogen, Alaska. Earth Planet. Sci. Lett. 270, 13–24.

Biddle, K.T., Uliana, M.A., Mitchum, R.M.J., Fitzgerald, M.G., Wright, 1986. The stratigraphic and structural evolution of the central and eastern Magallanes Basin, southern South America. In: Allen, P.A., Homewood, P. (Eds.), Foreland Basins. Black well, Oxford, UK, pp. 41–61.

Blisniuk, P.M., Stern, L.a., Chamberlain, C.P., Idleman, B., Zeitler, P.K., 2005. Climatic and ecologic changes during Miocene surface uplift in the Southern Patagonian Andes. Earth Planet. Sci. Lett. 230, 125–142.

Brandon, M.T., Roden-Tice, M., Garver, J.I., 1998. Late Cenozoic exhumation of the Cascadia accretionary wedge in the Olympic Mountains, northwest Washington State. Geol. Soc. Am. Bull. 110, 985–1009.

Breitsprecher, K., Thorkelson, D.J., 2009. Neogene kinematic history of Nazca–Antarctic–Phoenix slab windows beneath Patagonia and the Antarctic Peninsula. Tectonophysics 464, 10–20.

Calderón, M., Fildani, A., Hervé, F., Fanning, C.M., Weislogel, A., Cordani, U., 2007. Late Jurassic bimodal magmatism in the northern sea-floor remnant of the

Rocas Verdes basin, southern Patagonian Andes. J. Geol. Soc. London 164, 1011–1022.
Calderón, M., Fosdick, J.C., Warren, C., Massonne, H.-J., Fanning, C.M., Cury, L.F., Schwanethal, J., Fonseca, P.E., Galaz, G., Gaytán, D., Hervé, F., 2012. The low-grade Canal de las Montañas Shear Zone and its role in the tectonic emplacement of the Sarmiento Ophiolitic Complex and Late Cretaceous Patagonian Andes orogeny, Chile. Tectonophysics 524–525, 165–185.
Cande, S.C., Leslie, R.B., 1986. Late Cenozoic tectonics of the Southern Chile Trench. J. Geophys. Res. 91, 471–496.
Cembrano, J., Schermer, E., Lavenu, A., Sanhueza, A., 2000. Contrasting nature of deformation along an intra-arc shear zone, the Liquiñe–Ofqui fault zone, southern Chilean Andes. Tectonophysics 319, 129–149.
Clapperton, C., 1989. Asymmetrical drumlins in Patagonia, Chile. Sediment. Geol. 62, 387–398.
Covault, J.a., Romans, B.W., Graham, S.a., 2009. Outcrop expression of a continental-margin-scale shelf-edge delta from the Cretaceous Magallanes Basin, Chile. J. Sediment. Res. 79, 523–539.
Cruz, L., Teyssier, C., Perg, L., Take, A., Fayon, A., 2008. Deformation, exhumation, and topography of experimental doubly-vergent orogenic wedges subjected to asymmetric erosion. J. Struct. Geol. 30, 98–115.
Cruz, L., Malinski, J., Wilson, A., Take, W.A., Hilley, G.E., 2010. Erosional control of the kinematics and geometry of fold-and-thrust belts imaged in a physical and numerical sandbox. J. Geophys. Res. 115, 1–15.
Cunningham, W.D., Dalziel, I.W.D., Lee, T.Y., Lawver, L.A., 1995. Southernmost South America–Antarctic Peninsula relative plate motions since 84 Ma: implications for the tectonic evolution of the Scotia Arc region. J. Geophys. Res. 100, 8257–8266.
Dahlen, F.A., 1984. Noncohesive critical coulomb wedges: an exact solution. J. Geophys. Res. 89, 10125–10133.
Dahlen, F.A., Suppe, J., 1988. Mechanics, growth, and erosion of mountain belts. In: Clark Jr., S.P., Burchfield, B.C., Suppe, J. (Eds.), Processes in Continental Lithospheric Deformation. Geological Society of America, pp. 161–178.
Dalziel, I.W.D., de Wit, M.J., Palmer, K.F., 1974. Fossil marginal basin in the southern Andes. Nature 250, 291–294.
Davis, D., Suppe, J., Dahlen, F.A., 1983. Mechanics of fold-and-thrust belts and accretionary wedges. J. Geophys. Res. 88, 1153–1172.
DeCelles, P.G., DeCelles, P.C., 2001. Rates of shortening, propagation, underthrusting, and flexural wave migration in continental orogenic systems. Geology 29, 135.
Eagles, G., Livermore, R.A., Fairhead, J.D., Morris, P., 2005. Tectonic evolution of the west Scotia Sea. J. Geophys. Res. 110, http://dx.doi.org/10.1029/2004JB003154.
Ehlers, T.A., Farley, K.A., 2003. Apatite (U–Th)/He thermochronometry: methods and applications to problems in tectonic and surface processes. Earth Planet. Sci. Lett. 206, 1–14.
Ehlers, T.A., 2005. Crustal thermal processes and the interpretation of thermochronometer data. Rev. Mineral. Geochem. 58, 315–350.
Farley, K.A., 2000. Helium diffusion from apatite: general behavior as illustrated by Durango fluorapatite. J. Geophys. Res. 105, 2903–2914.
Farley, K.A., 2002. (U–Th)/He dating: techniques, calibrations, and applications. Rev. Mineral. Geochem. 47, 819–844.
Fanning, C.M., Hervé, F., Pankhurst, R.J., Rapela, C.W., Kleiman, L.E., Yaxley, G.M., Castillo, P., 2011. Lu–Hf isotope evidence for the provenance of Permian detritus in accretionary complexes of western Patagonia and the northern Antarctic Peninsula region. J. S. Am. Earth Sci. 32, 485–496.
Fildani, A., Cope, T.D., Graham, S.A., Wooden, J.L., 2003. Initiation of the Magallanes foreland basin: timing of the southernmost Patagonian Andes orogeny revised by detrital zircon provenance analysis. Geology 31, 1081–1084.
Fildani, A., Hessler, A.M., 2005. Stratigraphic record across a retroarc basin inversion: Rocas Verdes–Magallanes Basin, Patagonian Andes, Chile. Geol. Soc. Am. Bull. 117, 1596.
Fildani, A., Romans, B.W., Fosdick, J.C., Crane, W.H., Hubbard, S.M., 2008. Orogenesis of the Patagonian Andes as reflected by basin evolution in southernmost South America. Ariz. Geol. Soc. Dig. 22, 259–268.
Flowers, R.M., Ketcham, R.A., Shuster, D.L., Farley, K.A., 2009. Apatite (U–Th)/He thermochronometry using a radiation damage accumulation and annealing model. Geochim. Cosmochim. Acta 73, 2347–2365.
Fosdick, J.C., 2012. Linking orogenic deformation, exhumation, and basin evolution in the Patagonian Andes and Magallanes Basin, southernmost South America (Ph.D. Thesis). Stanford, Stanford University, 274 pp.
Fosdick, J.C., Romans, B.W., Fildani, A., Bernhardt, A., Calderón, M., Graham, S.A., 2011. Kinematic evolution of the Patagonian retroarc fold-and-thrust belt and Magallanes foreland basin, Chile and Argentina, 51°30′S. Geol. Soc. Am. Bull. 123, 1679–1698.
Fromm, R., Zandt, G., Beck, S.L., 2004. Crustal thickness beneath the Andes and Sierras Pampeanas at 30°S inferred from Pn apparent phase velocities. Geophys. Res. Lett. 31, L06625, http://dx.doi.org/10.1029/2003GL019231.
Ghiglione, M., Ramos, V., 2005. Progression of deformation and sedimentation in the southernmost Andes. Tectonophysics 405, 25–46.
Glasser, N.F., Jansson, K.N., 2005. Fast-flowing outlet glaciers of the Last Glacial Maximum Patagonian Icefield. Quat. Res. 63, 206–211.
Gorring, M.L., Kay, S.M., Zeitler, P.K., Ramos, V.A., Rubiolo, D., Fernandez, M.I., Panza, J.L., 1997. Neogene Patagonian plateau lavas: continental magmas associated with ridge collision at the Chile Triple Junction. Tectonics 16, 1–17.
Guenthner, W.R., Barbeau, D.L., Reiners, P.W., Thomson, S.N., 2010. Slab window migration and terrane accretion preserved by low-temperature thermochronology of a magmatic arc, northern Antarctic Peninsula. Geochem. Geophys. Geosyst. 11, 1–13.
Hamza, V.M., Muñoz, M., 1996. Heat flow map of South America. Geothermics 25, 599–621.
Harambour, S.M., 2002. Deep-seated thrusts in the frontal part of the Magallanes fold and thrust belt, Ultima Esperanza, Chile. 15th Congreso Geológico Argentino Actas 3, 232.
Hervé, F., Fanning, C.M., Pankhurst, R.J., 2003. Detrital zircon age patterns and provenance of the metamorphic complexes of southern Chile. J. S. Am. Earth Sci. 16, 107–123.
Hervé, F., Pankhurst, R.J., Fanning, C.M., Calderón, M., Yaxley, G.M., 2007a. The South Patagonian batholith: 150 my of granite magmatism on a plate margin. Lithos 97, 373–394.
Hervé, F., Massonne, H.-J., Calderón, M., Theye, T., 2007b. Metamorphic P–T conditions of Late Jurassic rhyolites in the Magallanes fold and thrust belt, Patagonian Andes, Chile. J. Iber. Geol. 33, 5–16.
Hilley, G.E., Strecker, M.R., 2004. Steady state erosion of critical Coulomb wedges with applications to Taiwan and the Himalaya. J. Geophys. Res. 109, http://dx.doi.org/10.1029/2002JB002284.
Hilley, G.E., Coutand, I., 2010. Links between topography, erosion, rheological heterogeneity, and deformation in contractional settings: insights from the central Andes. Tectonophysics 495, 78–92.
Hinojosa, L.F., Villagran, C., 1997. Historia de los bosques del sur de Sudamérica, I: antecedents paleobotánicos, geológicos y climáticos del Terciario del cono sur de América. Rev. Chil. Hist. Nat. 70, 225–239.
Horton, B.K., 1999. Erosional control on the geometry and kinematics of thrust belt development in the central Andes. Tectonics 18, 1292–1304.
Hourigan, J., Reiners, P., Brandon, M., 2005. U–Th zonation-dependent alpha-ejection in (U–Th)/He chronometry. Geochim. Cosmochim. Acta 69, 3349–3365.
Hubbard, S.M., Romans, B.W., Graham, S.A., 2008. Deep-water foreland basin deposits of the Cerro Toro Formation, Magallanes basin, Chile: architectural elements of a sinuous basin axial channel belt. Sedimentology 55, 1333–1359.
Kaplan, M.R., Hein, A.S., Hubbard, A., Lax, S.M., 2009. Can glacial erosion limit the extent of glaciation? Geomorphology 103, 172–179.
Katz, H.R., 1963. Revision of Cretaceous stratigraphy in Pata gonian cordillera of Ultima Esperanza, Magallanes Province, Chile. Am. Assoc. Pet. Geol. Bull. 47, 506–524.
Ketcham, R.A., 2005. Forward and inverse modeling of low-temperature thermochronometry data. Rev. Mineral .Geochem. 58, 275–314.
Klepeis, K.A., 1994. Relationship between uplift of the metamorphic core of the southernmost Andes and shortening in the Magallanes foreland fold and thrust belt, Tierra del Fuego, Chile. Tectonics 13, 882–904.
Klepeis, K., Betka, P., Clarke, G., Fanning, M., Hervé, F., Rojas, L., Mpodozis, C., Thomson, S., 2010. Continental underthrusting and obduction during the Cretaceous closure of the Rocas Verdes rift basin, Cordillera Darwin, Patagonian Andes. Tectonics 29, TC3014.
Kohn, M.J., Spear, F.S., Harrison, T.M., Dalziel, I.W.D., 1995. 40Ar/39Ar geochronology and P–T–t paths from the Cordillera Darwin metamorphic complex, Tierra del Fuego, Chile. J. Metamorph. Geol. 13, 251–270.
Koons, P.O., 1989. The topographic evolution of collisional mountain belts: a numerical look at the Southern Alps, New Zealand. Am. J. Sci. 289, 1041–1069.
Koons, P.O., Zeitler, P.K., Chamberlain, C.P., Craw, D., Meltzer, A.S., 2002. Mechanical links between erosion and metamorphism in Nanga Parbat, Pakistan Himalaya. Am. J. Sci. 302, 749–773.
Kraemer, P.E., 1998. Structure of the Patagonian Andes: regional balanced cross section at 50°S, Argentina. Int. Geol. Rev. 40, 896–915.
Kraemer, P.E., 2003. Orogenic shortening and the origin of the Patagonian orocline (56°S Lat). J. S. Am. Earth Sci. 15, 731–748.
Lagabrielle, Y., Goddéris, Y., Donnadieu, Y., Malavieille, J., Suárez, M., 2009. The tectonic history of Drake Passage and its possible impacts on global climate. Earth Planet. Sci. Lett. 279, 197–211.
Lagabrielle, Y., Scalabrino, B., Suárez, M., Ritz, J.-F., 2010. Mio-Pliocene glaciations of Central Patagonia: new evidence and tectonic implications. Andean Geol. 37, 276–299.
Lawrence, J.F., Wiens, D.A., 2004. Combined receiver-function and surface wave phase-velocity inversion using a Niching Genetic Algorithm: application to Patagonia. Bull. Seismol. Soc. Am. 94, 977–987.
Legates, D.R., Willmott, C.J., 1990. Mean seasonal and spatial variability in gauge-corrected, global precipitation. Int. J. Climatol. 10, 111–127.
Livermore, R., Hillenbrand, C.-D., Meredith, M., Eagles, G., 2007. Drake Passage and Cenozoic climate: an open and shut case? Geochem. Geophys. Geosyst. 8, http://dx.doi.org/10.1029/2005GC001224.
Lock, J., Willett, S., 2008. Low-temperature thermochronometric ages in fold-and-thrust belts. Tectonophysics 456, 147–162.
Malumián, N., Caramés, A., 1997. Upper Campanian–Paleogene from the Río Turbio coal measures in southern Argentina: micropaleontology and the Paleocene/Eocene boundary. J. S. Am. Earth Sci. 10, 189–201.
Malumián, N., Panza, J.L., Parisi, C., Nañez, C., Caramés, A., Torre, A., 2000. Hoja Geológica 5172-III, Yacimiento Río Turbio (1:250,000). Serv. Geol. Min. Argent. Bol. 247, 180.
Massonne, H.-J., Hervé, F., Calderón, M., Theye, T., 2004. Magmatic muscovite and garnet in granites of the South Patagonian Batholith. Boll. Geofís. Teor. Appl. 45, 121–125.
McQuarrie, N., Ehlers, T.A., Barnes, J.B., Meade, B., 2008. Temporal variation in climate and tectonic coupling in the central Andes. Geology 36, 999–1002.
Melnick, D., Echtler, H.P., 2006. Inversion of forearc basins in south-central Chile caused by rapid glacial age trench fill. Geology 34, 709.

Mercer, J.H., Sutter, J.F., 1982. Late Miocene–earliest Pliocene glaciation in southern Argentina; implications for global ice-sheet history. Atlantic 38, 185–206.
Metcalf, J.R., Fitzgerald, P.G., Baldwin, S.L., Muñoz, J.-A., 2009. Thermochronology of a convergent orogen: constraints on the timing of thrust faulting and subsequent exhumation of the Maladeta Pluton in the Central Pyrenean Axial Zone. Earth Planet. Sci. Lett. 287, 488–503.
Michael, P.J., 1984. Chemical differentiation of the Cordillera Paine granite (southern Chile) by in situ fractional crystallization. Contrib. Mineral. Petrol. 87, 179–195.
Michel, J., Baumgartner, L., Putlitz, B., Schaltegger, U., Ovtcharova, M., 2008. Incremental growth of the Patagonian Torres del Paine laccolith over 90 k.y. Geology 36, 459–462.
Montgomery, D.R., Balco, G., Willett, S.D., 2001. Climate, tectonics, and the morphology of the Andes. Geology 29, 579–582.
Moore, D.M., 1983, Flora of Tierra del Fuego. Anthony Nelson, Shropshire, 396 pp.
Natland, M.L., Gonzalez, P.E., Canon, A., Ernst, M., 1974. A system of stages for correlation of Magallanes Basin sediments. Am. Assoc. Pet. Geol. Mem. 139, 126.
Pardo-Casas, F., Molnar, P., 1987. Relative motion of the Nazca (Farallon) and South American Plates since Late Cretaceous time. Tectonics 6, 233–248.
Parras, A., Griffin, M., Feldmann, R., Casadío, S., Schweitzer, C., Marenssi, S., 2008. Correlation of marine beds based on Sr- and Ar-date determinations and faunal affinities across the Paleogene/Neogene boundary in southern Patagonia, Argentina. J. S. Am. Earth Sci. 26, 204–216.
Pascual, R., Ortiz Jaureguizar, E., 1990. Evolving climates and mammal faunas in Cenozoic South America. J. Hum. Evol 19, 23–60.
Poage, M.A., Chamberlain, C.P., 2002. Stable isotopic evidence for a Pre-Middle Miocene rain shadow in the western Basin and Range: implications for the paleotopography of the Sierra Nevada. Tectonics 21, 1–10.
Polonia, A., Torelli, L., Brancolini, G., Loreto, M.-F., 2007. Tectonic accretion versus erosion along the southern Chile trench: oblique subduction and margin segmentation. Tectonics 26, TC3005, http://dx.doi.org/10.1029/2006TC001983.
Putlitz, B., Baumgartner, L., Oberhänsli, R., Diamond, L., Altenberger, U., 2001. The Torres del Paine laccolith (Chile): intrusion and metamorphism. In: XI Annual V.M. Goldschmidt Conference Proceedings abs. 3534.
Radic, J.P., Mpodozis, C., Alvarez, P., 2007. Tectonic evolution of the Magallanes Fold and Thrust Belt between Seno Skyring and Peninsula Brunswick, southernmost Andes. In: GEOSUR 2007 International Congress, Santiago, Chile.
Rabassa, J., Coronato, A., Salemme, M., 2005. Chronology of the Late Cenozoic Patagonian glaciations and their correlation with biostratigraphic units of the Pampean region (Argentina). J. S. Am. Earth Sci. 20, 81–103.
Rabassa, J., 2008. Late Cenozoic Glaciations in Patagonia and Tierra del Fuego. Dev. Quat. Sci. 11, 151–204.
Ramírez de Arellano, C., Putlitz, B., Müntener, O., Ovtcharova, M., 2012. High precision U/Pb zircon dating of the Chaltén Plutonic Complex (Cerro Fitz Roy, Patagonia) and its relationship to arc migration in the southernmost Andes. Tectonics 31, http://dx.doi.org/10.1029/2011TC003048.
Ramos, V.A., 1989. Andean foothills structures in Northern Magallanes Basin, Argentina. Am. Assoc. Pet. Geol. Bull. 73, 887–903.
Ramos, V.A., 2005. Seismic ridge subduction and topography: foreland deformation in the Patagonian Andes. Tectonophysics 399, 73–86.
Ramos, V.A., Kay, S.M., 1992. Southern Patagonian plateau basalts and deformation: backarc testimony of ridge collisions. Tectonophysics 205, 261–282.
Ramos, V.A., Niemeyer, H., Skarmeta, J., Muñoz, J., 1982. Magmatic evolution of the Austral Patagonian Andes. Earth Sci. Rev. 18, 411–443.
Rapalini, A.E., Calderón, M., Singer, S., Hervé, F., Cordani, U., 2008. Tectonic implications of a paleomagnetic study of the Sarmiento Ophiolitic Complex, southern Chile. Tectonophysics 452, 29–41.
Reiners, P.W., Ehlers, T.A, Mitchell, S.G., Montgomery, D.R., 2003. Coupled spatial variations in precipitation and long-term erosion rates across the Washington Cascades. Nature 426, 645–647.
Reiners, P.W., Spell, T.L., Nicolescu, S., Zanetti, K.A., 2004. Zircon (U–Th)/He thermochronometry: He diffusion and comparisons with 40Ar/39Ar dating. Geochim. Cosmochim. Acta 68, 1857–1887.
Reiners, P.W., Brandon, M.T., 2006. Using thermochronology to understand orogenic erosion. Annu. Rev. Earth Planet. Sci. 34, 419–466.
Robertson Maurice, S.D., Wiens, D.A., 2003. Crustal and upper mantle structure of southernmost South America inferred from regional waveform inversion. J. Geophys. Res. 108, http://dx.doi.org/10.1029/2002JB001828.
Roe, G.H., 2005. Orographic Precipitation. Annu. Rev. Earth Planet. Sci. 33, 645–671.
Romans, B.W., Fildani, A., Hubbard, S.M., Covault, J.A., Fosdick, J.C., Graham, S.A., 2011. Evolution of deep-water stratigraphic architecture, Magallanes Basin, Chile. Mar. Pet. Geol. 28, 612–628.
Sánchez, A., Hervé, F., Saint-blanquat, M.D., 2008. Relations between plutonism in the back-arc region in southern Patagonia and Chile Rise subduction: a geochronological review. In: Proceedings of the 7th International Symposium on Andean Geodynamics. pp. 485–488.
Sanders, A.E., Andriessen, P.A.M., Cloetingh, S.A.P.L., 1999. Life cycle of the East Carpathian orogen: erosion history of a doubly vergent critical wedge assessed by fission track thermochronology. J. Geophys. Res. 104, 29095–29112.
Scalabrino, B., Ritz, J.-F., Lagabrielle, Y., 2011. Relief inversion triggered by subduction of an active spreading ridge: evidence from glacial morphology in Central Patagonia. Terra Nova 23, 63–69.
SEGEMAR, 1997. Mapa geológico de la República Argentina, escala 1:2.500.000. Servicio Geológico Minero Argentino.
SERNAGEOMIN, 2003. Mapa Geológico de Chile: version digital. publicación geológica digital, No. 4, 2003. CDROM, versión 1.0, 2003. Base Geológica escala 1:1.000.000. Gobierno de Chile, Servicio Nacional de Geología y Minería, Subdirección Nacional de Geología.
Sobel, E.R., Strecker, M.R., 2003. Uplift, exhumation and precipitation: tectonic and climatic control of Late Cenozoic landscape evolution in the northern Sierras Pampeanas, Argentina. Basin Res. 15, 431–451.
Solari, M., Le Roux, J., Hervé, F., Airo, A., Calderón, M., 2012. Evolution of the Great Tehuelche Paleolake in the Torres del Paine National Park of Chilean Patagonia during the Last Glacial Maximum and Holocene. Andean Geol. 39 (1), 1–21.
Stern, L.A., Blisniuk, P.M., 2002. Stable isotope composition of precipitation across the southern Patagonian Andes. J. Geophys. Res. 107, http://dx.doi.org/10.1029/2002JD002509.
Stock, J.D., Montgomery, D.R., 1999. Geologic constraints on bedrock river incision using the stream power law. J. Geophys. Res. 104, 4983–4993.
Strecker, M.R., Alonso, R.N., Bookhagen, B., Carrapa, B., Hilley, G.E., Sobel, E.R., Trauth, M.H., 2007. Tectonics and Climate of the Southern Central Andes. Annu. Rev. Earth Planet. Sci. 35, 747–787.
Suárez, M., 1976. La Cordillera Patagónica, su división y relación con la Peninsula Antárctica. An. Institudo de la Patagonia 7, 105–113.
Suárez, M., de la Cruz, R., Bell, C.M., 2000. Timing and origin of deformation along the Patagonian fold and thrust belt. Geol. Mag. 137, 345–353.
Thiede, R., et al., 2005. From tectonically to erosionally controlled development of the Himalayan orogen. Geology 33, 689–692.
Thomson, S.N., 2002. Late Cenozoic geomorphic and tectonic evolution of the Patagonian Andes between latitudes 42°S and 46°S: an appraisal based on fission-track results from the transpressional intra-arc Liquiñe-Ofqui fault zone. Geol. Soc. Am. Bull. 114, 1159–1173.
Thomson, S.N., Hervé, F., Stöckhert, B., 2001. Mesozoic–Cenozoic denudation history of the Patagonian Andes (southern Chile) and its correlation to different subduction processes. Tectonics 20, 693–711.
Thomson, S.N., Brandon, M.T., Tomkin, J.H., Reiners, P.W., Vásquez, C., Wilson, N.J., 2010. Glaciation as a destructive and constructive control on mountain building. Nature 467, 313–317.
Tomkin, J.H., 2007. Coupling glacial erosion and tectonics at active orogens: a numerical modeling study. J. Geophys. Res. 112, 1–14.
Tomkin, J.H., Braun, J., 2002. The influence of alpine glaciation on the relief of tectonically active mountain belts. Am. J. Sci. 302, 169–190.
Ton-That, T., Singer, B.S., Morner, N.-A., Rabassa, J., 1999. Datación de lavas basálticas por Ar/Ar y geología glacial de la región del lago Buenos Aires, Provincia de Santa Cruz, Argentina. Rev. Asoc. Geol. Argent. 54, 333–352.
Uba, C.E., Kley, J., Strecker, M.R., Schmitt, A.K., 2009. Unsteady evolution of the Bolivian Subandean thrust belt: the role of enhanced erosion and clastic wedge progradation. Earth Planet. Sci. Lett. 281, 134–146.
Wenzens, G., 2006. Terminal moraines, outwash plains, and lake terraces in the vicinity of Lago Cardiel (49°S; Patagonia, Argentina)—evidence for Miocene foreland glaciations. Arct. Antarct. Alp. Res. 38, 276–291.
Whipple, K., Meade, B., 2006. Orogen response to changes in climatic and tectonic forcing. Earth Planet. Sci. Lett. 243, 218–228.
Willett, S.D., 1999. Orogeny and orography: the effects of erosion on the structure Processes. J. Geophys. Res. 104, 28957–28981.
Willett, S., Beaumont, C., Fullsack, P., 1993. Mechanical model for the tectonics of doubly vergent compressional orogens. Geology 21, 371–374.
Willett, S.D., Brandon, M.T., 2002. On steady states in mountain belts. Geology 30, 175–178.
Wilson, T.J., 1991. Geological Society of America Bulletin Transition from back-arc to foreland basin development in the southernmost. Geol. Soc. Am. Bull. 103, 98–111.
Wobus, C.W., Hodges, K.V., Whipple, K.X., 2003. Has focused denudation sustained active thrusting at the Himalayan topographic front? Geology 31, 861–864.
Wolf, R.A., Farley, K.A., Silver, L.T., 1996. Helium diffusion and low-temperature thermochronometry of apatite. Geochim. Cosmochim. Acta 60, 4231–4240.
Yuan, X., Kind, R., Li, X., Wang, R., 2006. The S receiver functions: synthetics and data example. Geophys. J. Int. 165, 555–564.
Zachos, J., Pagani, M., Sloan, L., Thomas, E., Billups, K., 2001. Trends, rhythms, and aberrations in global climate 65 Ma to present. Science 292, 686–693.
Zandt, G., Velasco, A.A., Beck, S.L., 1994. Composition and thickness of the southern Altiplano crust, Bolivia. Geology 22, 1003–1006.
Zeitler, P.K., 1985. Cooling history of the NW Himalaya, Pakistan. Tectonics 4, 127–151.
Zeitler, P.K., Herczeg, A.L., McDougall, I., Honda, M., 1987. U–Th–He dating of apatite: a potential thermochronometer. Geochim. Cosmochim. Acta 51, 2865–2868.